AD-A061 139 NAVAL OCEAN SYSTEMS CENTER SAN DIEGO CA F/G 9/3
ADAPTIVE LINE ENHANCER USED FOR SPECTRAL RESOLUTION, ALE RESOLU--ETC(U)
AUG 78 J G MELVILLE

UNCLASSIFIED NOSC/TR-281 NL

1 OF 1
AD
A061139

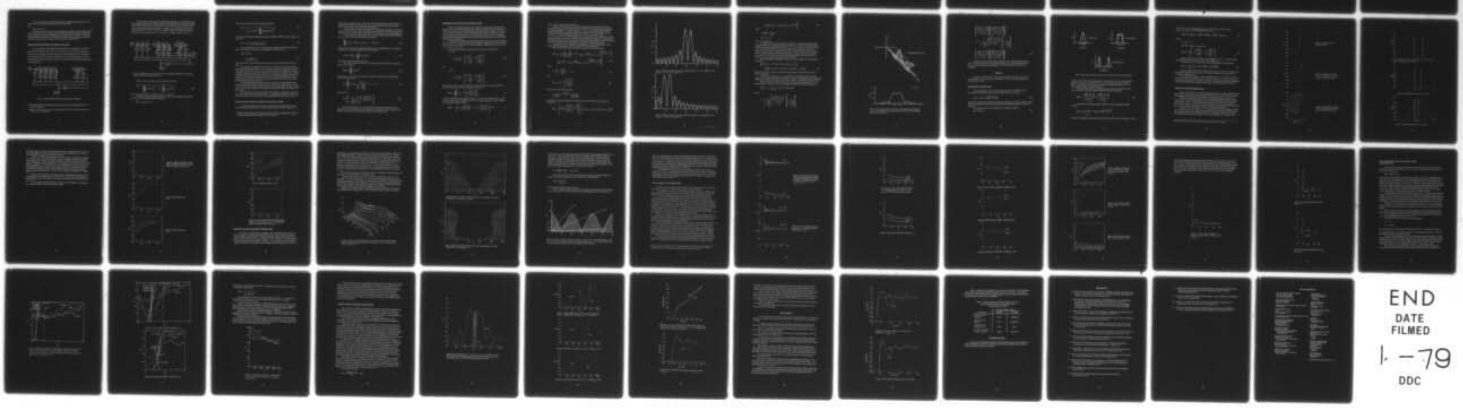

END
DATE
FILMED
1-79
DDC

LEVEL

NOSC

NOSC TR 281

Technical Report 281
Oct 77 - May 78

ADAPTIVE LINE ENHANCER USED FOR SPECTRAL RESOLUTION

ALE resolution of two sinusoids in the presence of white noise is determined for various filter and signal parameters.

J. G. Melville
JG Melville

3 August 1978

Research and Development: October 1977 - May 1978

Prepared for
Naval Electronic Systems Command
Washington, DC 20360

53p.

NOSC/TR-281

F11121

NAVAL OCEAN SYSTEMS CENTER
SAN DIEGO, CALIFORNIA 92152

NAVAL OCEAN SYSTEMS CENTER, SAN DIEGO, CA 92152

AN ACTIVITY OF THE NAVAL MATERIAL COMMAND

RR GAVAZZI, CAPT, USN
Commander

HL BLOOD
Technical Director

ADMINISTRATIVE INFORMATION

Work was performed as part of the NOSC New Professional Program under 62711N, XF11-121, by members of the Electronics Division of the Fleet Engineering Department. It was sponsored by the Naval Electronic Systems Command (Code 320). This report covers work from October 1977 to May 1978 and was approved for publication 3 August 1978.

Released by
RH Hearn, Head
Electronics Division

Under authority of
DA Kunz, Head
Fleet Engineering Department

UNCLASSIFIED

SECURITY CLASSIFICATION OF THIS PAGE *(When Data Entered)*

REPORT DOCUMENTATION PAGE

READ INSTRUCTIONS BEFORE COMPLETING FORM

1. REPORT NUMBER: NOSC Technical Report 281 (TR 281)

2. GOVT ACCESSION NO.

3. RECIPIENT'S CATALOG NUMBER

4. TITLE *(and Subtitle)*

ADAPTIVE LINE ENHANCER USED FOR SPECTRAL RESOLUTION

ALE resolution of two sinusoids in the presence of white noise is determined for various filter and signal parameters

5. TYPE OF REPORT & PERIOD COVERED: Research and Development, October 1977-May 1978

6. PERFORMING ORG. REPORT NUMBER

7. AUTHOR(s)

JG Melville

8. CONTRACT OR GRANT NUMBER(s)

9. PERFORMING ORGANIZATION NAME AND ADDRESS

Naval Ocean Systems Center
San Diego CA 92152

10. PROGRAM ELEMENT, PROJECT, TASK AREA & WORK UNIT NUMBERS: 62711N, XF11-121

11. CONTROLLING OFFICE NAME AND ADDRESS

Naval Electronic Systems Command (Code 320)
Washington DC 20360

12. REPORT DATE: 3 August 1978

13. NUMBER OF PAGES: 48

14. MONITORING AGENCY NAME & ADDRESS *(if different from Controlling Office)*

15. SECURITY CLASS. *(of this report)*: Unclassified

15a. DECLASSIFICATION/DOWNGRADING SCHEDULE

16. DISTRIBUTION STATEMENT *(of this Report)*

Approved for public release; distribution unlimited

17. DISTRIBUTION STATEMENT *(of the abstract entered in Block 20, if different from Report)*

18. SUPPLEMENTARY NOTES

19. KEY WORDS *(Continue on reverse side if necessary and identify by block number)*

Adaptive signal processing
Linear filters
Spectral estimation techniques
Frequency resolution
Adaptive line enhancing
Adaptive filtering
Spectral resolution

20. ABSTRACT *(Continue on reverse side if necessary and identify by block number)*

ALE spectral resolution was analyzed by using the solutions for the converged ALE weight vector. The functions $|H(\omega)|$, $Q(\omega)$, and $S(\omega)$ each contain information pertaining to spectral resolution.

When the bulk delay, Δ, is greater than 1, both $|H(\omega)|$ and $S(\omega)$ experience more than one resolved-unresolved transition as the frequency separation between two sinusoids is decreased. This phenomemon is completely explained by the basic weight vector solution.

(Continued)

DD FORM 1 JAN 73 1473 EDITION OF 1 NOV 65 IS OBSOLETE
S/N 0102-014-6601 |

UNCLASSIFIED

SECURITY CLASSIFICATION OF THIS PAGE *(When Data Entered)*

20. Continued.

By Marple's criterion, the resolutions of $|H(\omega)|$ and $Q(\omega)$ were determined for various values of the filter length (L) and SNR. When the weight vector is known exactly, the $|H(\omega)|$ function provides better resolution than $Q(\omega)$, particularly at high SNR.

When the ALE weights contain noise, and particularly at high input SNR, $|H(\omega)|$ is superior to $Q(\omega)$ and $S(\omega)$ for spectral resolution (as shown by a Monte Carlo analysis) whereas $Q(\omega)$ and $S(\omega)$ are more accurate than $|H(\omega)|$ for determining sinusoid frequency.

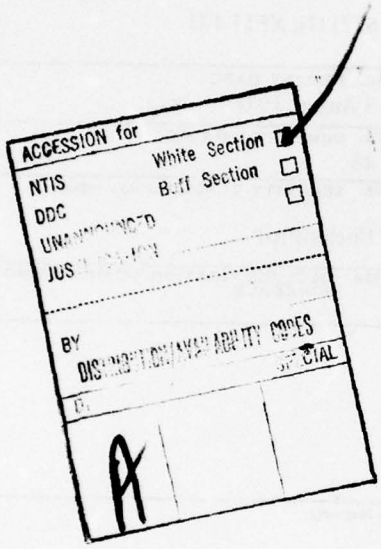

OBJECTIVE

Investigate the ability of the adaptive line enhancer to resolve two sinusoids of different frequency in the presence of white noise. Determine the frequency resolution for a variety of input signal-to-noise ratios and as a function of the various ALE parameters.

RESULTS

1. A modified maximum entropy spectrum, $S(\omega)$, having many of the desirable properties of $Q(\omega)$ can be formed from the ALE weight vector for $\Delta \neq 1$, where Δ is the bulk delay.

2. For $\Delta > 1$, both $|H(\omega)|$ and $S(\omega)$ have multiple regions of resolution, contrary to the concept of a simple limit of resolution.

3. The occurrence of multiple regions of resolution was explained simply in terms of a geometrical model for the weight vector.

4. The bulk delay, Δ, is the critical factor in determining the frequency bands which result in resolved spectra when multiple regions of resolution are present. The capability of arbitrary Δ adjustment permits the ALE to be "turned" to resolve a doublet with known frequency separation.

5. On the basis of Marple's criterion, the relative resolving capability of $|H(\omega)|$ proved to be the best when the weight vector is known exactly, followed by $S(\omega)$, then $Q(\omega)$. The superiority of $|H(\omega)|$ was most significant for high SNR. For SNR below 0 dB, each spectral function has essentially the same resolution.

6. For the same value of Δ, $S(\omega)$ has fewer problems caused by multiple regions of resolution than has $|H(\omega)|$.

7. When noise is added to the weight vector for a high SNR input, the effect on the ability of the ALE to resolve the two peaks is much worse for $Q(\omega)$ than for $|H(\omega)|$. For low-SNR inputs, the effect is about the same in both $Q(\omega)$ and $|H(\omega)|$, with a slight superiority of $Q(\omega)$ for some values of σ^2.

8. A plot of the location of spectral peaks in the functions $|H(\omega)|$ and $Q(\omega)$ shows that for higher SNR, the locations of the tonal frequencies correspond much more closely to the peaks of $Q(\omega)$ than to the peaks of $|H(\omega)|$. For low SNR, the performance of the two spectral estimators is about the same.

RECOMMENDATIONS

Continue the investigations initiated under this program to provide more definitive baseline performance bounds for two-sinusoid resolution capabilities for the various spectral estimators described in this report.

CONTENTS

INTRODUCTION

The adaptive line enhancer (ALE) has proven to be a useful tool in separating narrowband and broadband components in a variety of signal types (ref 1). The ALE is often used as a prefilter to signal processors that are used for spectral analysis of the narrowband portions of an input signal. It has been shown, however, that the ALE is itself a type of spectral estimator and can be used effectively to determine the number and frequencies of narrowband components in a given signal.

The specific goal of this task was to investigate the ability of the ALE to resolve two sinusoids of different frequency in the presence of white noise. Frequency resolution was to be determined for a variety of input signal-to-noise ratios and as a function of the various ALE parameters.

This report first offers a few general comments about adaptive signal processing and linear prediction filters. The ALE response to an input consisting of two sinusoids in white noise is developed by means of the exact solution (ref 2), for the ALE filter weights (ie, the ALE weight vector). Approximations to the exact solution are then made, yielding mathematical expressions highlighting the effects governing the limit of resolution. The exact solution is solved numerically to provide plots of resolution for a variety of ALE configurations and signal types. The effect of weight vector noise on ALE resolution is discussed, and the report concludes with a critical discussion of the strengths and weaknesses of the various spectral resolution techniques which use ALE weight vectors as their primary input data.

THEORETICAL BASIS

There are, in general, two ways of using an ALE to form a spectral estimate. This section establishes the theoretical basis for these techniques and develops some of their properties relating to the problem of spectral resolution.

The ALE was first developed as an instrument to separate various components of an input signal on the basis of bandwidth (ref 3), and specifically as an adaptive filter to pass only the narrowband portions of the signal. It was noted that the magnitude of the transfer function of the adaptive filter ($|H(\omega)|$) should contain peaks at frequencies corresponding to the narrowband components of the input. The correspondence forms the basis for what will be termed the magnitude of H or $|H(\omega)|$ spectral estimate. Treichler (ref 4) has studied

---

1. Widrow, B, Glover, JR, McCool, JM, Kaunitz, J, Williams, CS, Hearn, RH, Zeidler, JR, Dong, E, and Goodlin, RC, Adaptive Noise Cancelling: Principles and Applications, IEEE Proc, vol 63, p 1692-1716, December 1975
2. NOSC TR 193, Adaptive Enhancement of Multiple Sinusoids in Uncorrelated Noise, by JR Zeidler, EH Satorius, DM Chabries, and HT Wexler, 1 October 1977. Published later as The Performance of the Adaptive Line Enhancer for Multiple Sinusoidal Inputs in White Noise, IEEE Trans on Acoustics, Speech and Signal Processing, June 1978
3. NOSC Technical Report NUC TP 530, Principles and Applications of Adaptive Filters: A Tutorial Review, by JM McCool and B Widrow, March 1977
4. Treichler, J, The Spectral Line Enhancer, PhD dissertation, Dept of Electrical Engineering, Stanford University, Stanford CA, May 1977

this method of spectral estimation and found it to be highly biased. (In fact the designation "spectral estimator" might better be replaced by "spectral indicator.") The $|H(\omega)|$ spectrum does serve to indicate the number and frequencies of the narrowband components of the input signal and therefore may be useful in a variety of applications.

The second type of spectral estimate that can be performed by using an ALE is known as the maximum entropy spectral estimate (ref 5). This is an unbiased spectral estimate that converges to the precise input spectrum in the limit of a large number of ALE weights.

The goals of this section are first to provide a general theoretical background relating to the $|H(\omega)|$ and maximum entropy spectral estimates and second to examine the response of these spectral estimates to an input of two sinusoids in white noise by analyzing the mathematical equations governing their operation.

ADAPTIVE LINE ENHANCER

The principles of operation governing the ALE have been discussed at length in the open literature (ref 1–4). For the purpose of establishing notation, however, they are reviewed here.

The basic configuration of the ALE is shown in figure 1. The input signal X(j) experiences a bulk delay of Δ time steps and is then filtered by an L weight transversal filter whose weights have the values W(0) through W(L–1). The output of this filter

$$X'(j) = \sum_{\ell=0}^{L-1} X(j - \Delta - \ell)W(\ell) \quad . \tag{1}$$

The output is then subtracted from the current input signal to form an error signal

$$\epsilon(j) = X(j) - X'(j) \quad . \tag{2}$$

To minimize the power of the error signal $\epsilon(j)$, the ALE then automatically adjusts the weight vector by iteratively adjusting the ALE weights according to the well-known LMS algorithm (ref 6),

$$W_{j+1}(\ell) = W_j(\ell) + 2\mu\epsilon(j)X(j - \Delta - \ell) \quad . \tag{3}$$

The μ is an adjustable parameter which controls the rate of convergence of the weight vector $\underset{\sim}{W}$ to its steady state value, $\underset{\sim}{W}^{\star}$. When the adaptive filter is in its converged state, the output X'(j) includes only the portions of the input which are correlated for a time longer than Δ time steps.

---

5. Burg, JP, Maximum Entropy Spectral Analysis, paper presented at the 37th Annual International Meeting, Society of Exploration Geophysicists, Oklahoma City OK, 31 October 1967

6. Widrow, B, Adaptive Filters, in Aspects of Network and System Theory, R Kalman and N DeClaris, Ed, p 563-587, Holt, Rinehart, and Winston, New York NY, 1971

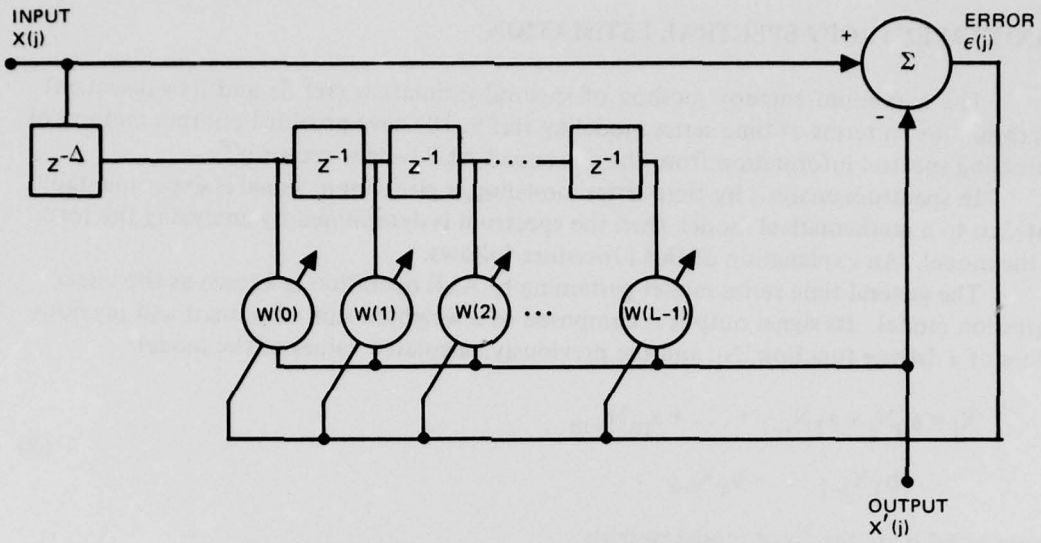

Figure 1. Adaptive line enhancer (ALE). The detailed procedure to update $W_j(\ell)$ from $\epsilon(j)$ is not explicitly shown.

The transfer function of the filter is calculated by performing a Fourier transform on the weight vector $\underset{\sim}{W}^{\star}$. The spectral information is inferred from the number and location of peaks in the magnitude of the transfer function $|H^{\star}(\omega)|$, where

$$H^{\star}(\omega) = \sum_{\ell=1}^{L-1} W^{\star}(\ell) e^{-j\omega(\ell+1)} \quad . \tag{4}$$

It has been shown that for the special case of multiple sinusoids in white noise, the weight vector $W^{\star}(\ell)$ is a weighted sum of sinusoids, corresponding in number and frequency to those of the input signal (ref 2). The amplitudes of these sinusoids are not independently related to the amplitudes of the input sinusoids; therefore $|H(\omega)|$ does not provide a complete spectral estimate of even the narrowband components of the input signal.

Where the noise background is not white and where the narrowband portions of the signal have significant bandwidth, analysis of the form of the weight vector is correspondingly more complex. Such considerations are topics of current research (ref 7, 8).

[redacted]R 231, Modified Maximum Entropy Spectral Analysis of Bandlimited Signals in Lowpass [redacted]T Alexander, 30 April 1978

8. N[redacted] 32, Linear Predictive Spectral Estimation of Bandlimited Signals in Lowpass Noise, by ST A[redacted]ler and EH Satorius, 31 March 1978

MAXIMUM ENTROPY SPECTRAL ESTIMATION

The maximum entropy method of spectral estimation (ref 5) and its subsequent interpretation in terms of time series modeling (ref 9, 10) have provided another method of extracting spectral information from the converged ALE weight vector $\underset{\sim}{W}^{\star}$.

In spectrum analysis by time series modeling, a given input signal is experimentally matched to a mathematical model, then the spectrum is determined by analyzing the form of the model. An explanation of this procedure follows.

The general time series model pertaining to ALE operation is known as the linear regression model. Its signal output is composed of a weighted sum of present and previous values of a driving function, N_j, and the previously calculated values of the model:

$$X_j = a_0 N_j + a_1 N_{j-1} + \ldots + a_m N_{j-m} - b_1 X_{j-1} \ldots - b_\ell X_{j-\ell} \quad , \tag{5}$$

where a and b are the fixed model weights.

One advantage of using this type of model is the straightforward determination of the spectrum of X_j from the values of the weights and a knowledge of the driving function, N_j.

With the definition $b_0 = 1$, equation 5 may be rewritten as

$$\sum_{k=0}^{\ell} b_k X_{j-k} = \sum_{k=0}^{m} a_k N_{j-k} \quad . \tag{6}$$

The Z-transform of equation 6 is as follows:

$$X(z)B(z) = A(z)N(z) \quad , \tag{7}$$

where

$$X(z) = \sum_{j=-\infty}^{\infty} X_j Z^{-j} \tag{8}$$

$$N(z) = \sum_{j=-\infty}^{\infty} N_j Z^{-j} \tag{9}$$

$$A(z) = \sum_{j=-\infty}^{\infty} a_j Z^{-j} \tag{10}$$

---

9. Van den Bos, A, Alternative Interpretation of Maximum Entropy Spectral Analysis, IEEE Trans on Information Theory, vol IT-17, p 493-494, July 1971

10. Ulrych, TJ, and Clayton, RW, Time Series Modelling and Maximum Entropy, Physics of the Earth and Planetary Interiors, vol 12, p 188-200, 1976

$$B(z) = \sum_{j=-\infty}^{\infty} b_j Z^{-j} \quad . \tag{11}$$

When Z is taken along the unit circle, the quantities $|X(z)|^2$ and $|N(z)|^2$ are respectively the power spectrum of the model signal, $S_x(z)$, and the power spectrum of the driving signal, $S_n(z)$. When the model is driven by a white noise sequence with power spectral density σ^2, the power spectrum of the model signal is given by

$$S_x(z) = \left| \frac{A(z)}{B(z)} \right|^2 \sigma^2 \quad . \tag{12}$$

That the spectrum of a linear regression model can be so easily expressed in terms of the model coefficients is of no avail unless the actual input data signals can also be adequately represented by such a model. The practical application of time series modeling also necessitates some method for determining the values of the model coefficients that best represent the input signal.

To help determine how these conditions can be met, it is convenient to refer separately to the a's and b's of equation 5. When all the b's are zero, the process described by that equation is known as a moving average (MA) process of order M + 1. When all the a's are zero, equation 5 results in an autoregressive (AR) process of order ℓ. The combination of these two models is often referred to as a mixed autoregressive moving average (ARMA) process.

The AR model is particularly well suited to the study of a narrowband signal since it can be shown that only 2N + 1 AR coefficients are needed to exactly model a signal consisting of N sinusoids (ref 11). It can be shown further that the process of N sinusoids in white noise can be represented exactly by an ARMA model with 2N + 1 AR coefficients and 2N + 1 MA coefficients (ref 11).

The complete generality of these models is achieved in the limiting case in which the orders of the models (ie, the number of coefficients) become infinite. As noted in ref 10, the Wold decomposition theorem (ref 12, 13) states that any nondeterministic stationary stochastic process with an absolutely continuous spectral distribution may be represented exactly by an MA model of possible infinite order. Further there generally exists an AR model which also represents the process. (For a discussion of specific details, see ref 10, 12, 13.)

While an AR, MA, or ARMA process may be used to model a given input signal, the number of parameters required for each model and the effort required to determine their numerical values from the input data can vary greatly. For example, a single sinusoid may be completely modeled by two AR coefficients whereas the corresponding MA representation requires an infinite number of terms. In general, a process can be represented with the fewest number of parameters by using an ARMA process (ref 14).

---

11. Marple, S, Conventional Fourier, Autoregressive, and Special ARMA Methods of Spectrum Analysis, engineering thesis, Dept of Electrical Engineering, Stanford University, Stanford CA, 1976

12. Wold, H, Bibliography on Time Series and Stochastic Processes, Oliver and Boyd, London, 1965

13. Koopmans, LH, The Spectral Analysis of Time Series, Academic Press, New York NY, 1974

14. Graupe, D, Krause, DJ, and Moore, JB, Identification of Autoregressive Moving-Average Parameters of Time Series, IEEE Trans on Automatic Control, vol AC-20, p 104-107, February 1975

Even though the ARMA model is the most economical in the number of weights needed to model a given input process, time series modeling is usually done by using AR models (ref 14) because solutions for AR parameters are simpler to obtain and are numerically more stable than the corresponding processes required to determine the optimum set of ARMA parameters. The process of determining the spectrum of stationary input signal X_j is demonstrated by analyzing the output of an ARMA filter driven by white noise:

$$N_j \rightarrow \frac{A(z)}{B(z)} \rightarrow X_j \quad .$$

The transfer function is given here by the quotient of the transfer functions of its component MA and AR parts, A(z)/B(z).

If X_j is passed through a second filter having a transfer function B(z)/A(z), the resultant output N_j' will have the same spectrum as N_j (white):

$$N_j \rightarrow \frac{A}{B} \rightarrow X_j \rightarrow \frac{B}{A} \rightarrow N_j' \quad .$$

In principle, the correct signal model can be determined by changing the parameters of the second filter until N_j' has a white spectrum. The input spectrum can then be estimated to be the Z-transform of the inverse of the transfer function of the optimum whitening filter.

As mentioned previously, practical considerations often require the whitening filter to be of the MA type. Symbolically this can be expressed as

$$X_j \rightarrow C(z) \rightarrow N_j'' \quad ,$$

where C(z) represents the transfer function of the MA filter (all-zero model) and the double-prime on N_j indicates that it may be slightly different from N_j'.

If C(z) were allowed to be of arbitrarily large order, by Wold's decomposition theorem C(z) could be formed such that A(z)/B(z) = 1/C(z) and N_j'' could be whitened:

$$N_j \rightarrow \frac{A(z)}{B(z)} \rightarrow X_j \rightarrow C(z) \rightarrow N_j \quad . \tag{13}$$

Equation 13 shows that such a process models the input X_j as an autoregressive process with a spectrum of 1/C(z).

When the length of the whitening filter is finite (or equivalently when $C_i = 0$ for i greater than some fixed integer), equation 13 is only approximately valid and C(z) represents the best finite order AR approximation to the given ARMA process, as determined by the whitening algorithm.

Once the optimum set of weights has been selected subject to the constraints $C_0 = 1$, $C_i = 0$, $i > L$, the maximum entropy spectral estimate may be defined as

$$S_x(e^{j\omega}) = \frac{\sigma^2}{\left| 1 + \sum_{k=1}^{L} c_k e^{-j\omega} \right|^2} \quad . \tag{14}$$

For the purpose of determining resolution, the normalized quantity $S_x(\omega)/\sigma^2$ will be referred to as the maximum entropy spectral estimate, $Q(\omega)$.

Thus

$$Q(\omega) = S_x(\omega)/\sigma^2 . \tag{15}$$

With respect to the problem at hand (resolution of multiple sinusoids in the presence of noise), $Q(\omega)$ is expected to perform well at high SNR since the actual input at high SNR closely resembles the process of multiple sinusoids, a process which is known to be exactly represented by an AR model. At low SNR the full ARMA model is required, and the result may be an inaccurate spectral estimate for the maximum entropy method.

MAXIMUM ENTROPY SPECTRUM FROM ALE WEIGHTS

Figure 2 shows an adaptive MA filter which might be used to produce a maximum entropy spectral estimate to the input X_j. Here the power of ϵ_j (ie, $\overline{\epsilon_j^2}$) has been taken as the criterion by which the relative whiteness of the output signal is measured. (References 15 and 16 discuss min $\overline{\epsilon_j^2}$ as a measure of whiteness.) The figure shows that the optimum set of MA filter weights (or equivalent AR model coefficients) could be determined by using the LMS algorithm.

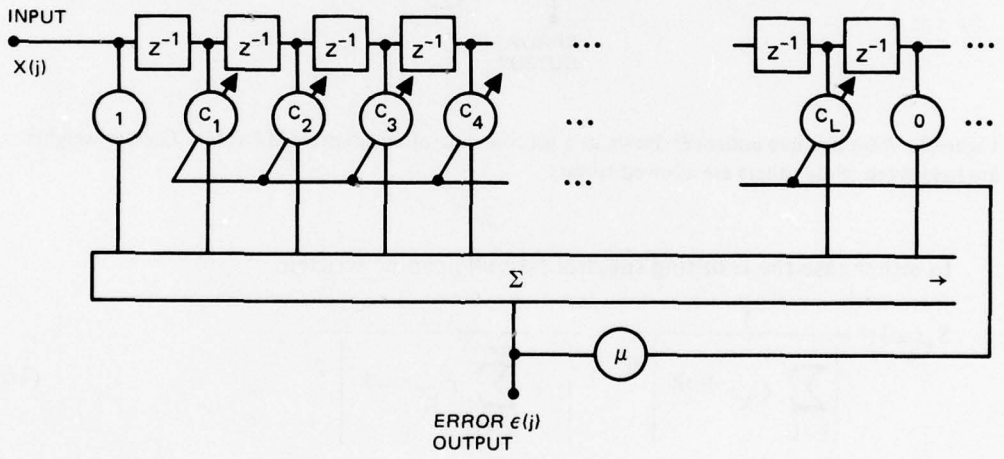

Figure 2. Adaptive MA filter with finite number of nonzero coefficients.

15. Peacock, K, and Treitel, S, Predictive Deconvolution: Theory and Practice, Geophysics, vol 34, p 155-169, April 1969

16. Kailath, T, A View of Three Decades of Linear Filtering Theory, IEEE Trans on Information Theory, vol IT-20, p 145-181, March 1974

Figure 3 shows an L-weight ALE operating with bulk delay, Δ. This diagram represents a process identical to that shown in figure 1 but rearranged in the format of an all-pole (AR) LMS spectral estimator to permit figures 2 and 3 to be viewed as special cases of an infinite order LMS AR spectral estimator. In figure 2, $\overline{\epsilon_j^2}$ is minimized, subject to the constraints that $C_0 = 1$ and $C_i = 0$ for $i > L$. The ALE represented in figure 3 minimizes $\overline{\epsilon_j^2}$ subject to the constraints $C_0 = 1$, $C_i = 0$ for $0 < i < \Delta$ and $C_i = 0$ for $i > \Delta + L - 1$.

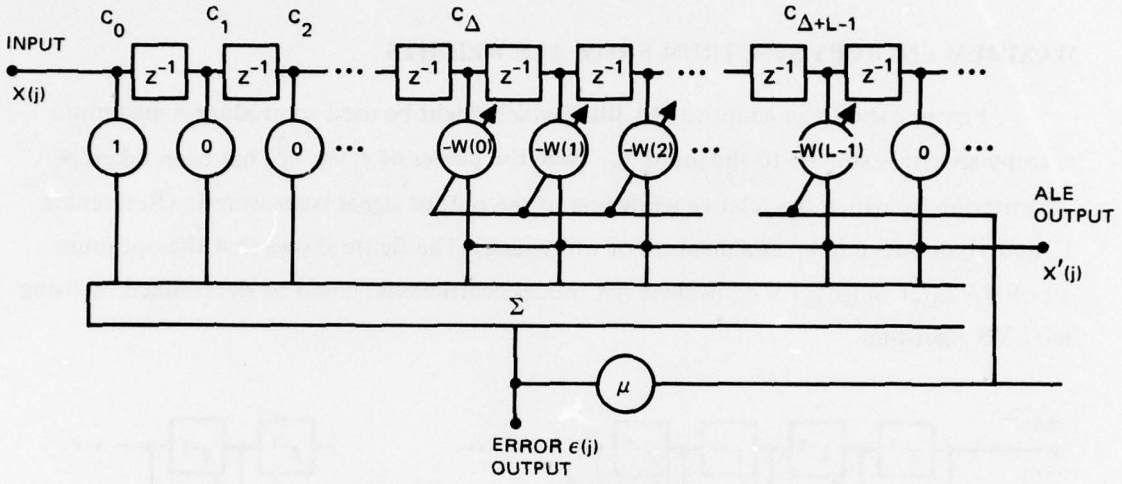

Figure 3. Adaptive line enhancer drawn as a specific case of an adaptive MA filter. Certain weights are held fixed while others are allowed to vary.

In either case the resulting spectral estimate can be written

$$S_x(\omega) = \frac{1}{\left| \sum_{k=0}^{\infty} C_k e^{-j\omega k} \right|^2} = \frac{1}{\left| 1 + \sum_{k=1}^{\infty} C_k e^{-j\omega k} \right|^2} \quad . \tag{16}$$

This is the direct extension of equation 15 for $L \to \infty$ and $\sigma^2 = 1$.

By using the following relationship (fig 3) between the autoregressive model parameters C_j and the corresponding ALE weights W_j,

$$W(i) = -C_{\Delta+1} \text{ for } i > 0 \quad .$$

Equation 16 can be shown to have the following form:

$$S_x(\omega) = \frac{1}{\left| 1 - e^{-j\omega(\Delta-1)} \sum_{j=0}^{L-1} W(j) e^{-j\omega(j+1)} \right|^2} \quad . \tag{17}$$

This expression is further simplified by using the definition of $H^{\star}(\omega)$ given in equation 4, to show that

$$S_x(\omega) = \frac{1}{\left| 1 - e^{-j\omega(\Delta-1)} H^{\star}(\omega) \right|^2} \quad . \tag{18}$$

For the special case of $\Delta = 1$, $S_x(\omega)$ is the maximum entropy spectral estimate $Q(\omega)$, and equation 18 assumes the form suggested by Griffiths (ref 17):

$$S_x(\omega) = Q(\omega)$$

$$= \frac{1}{\left| 1 - H^{\star}(\omega) \right|^2} \quad . \tag{19}$$

As noted previously, this estimator converges to the true input spectrum in the limit of large L.

This important convergence property does not hold for the spectral estimates formed from ALE weights where $\Delta \neq 1$, as in figure 3. Equation 16 shows that the first few AR weights contribute to features in the spectral estimate $S(\omega)$ which have the largest spread in frequency (ie, which are broadband). As Δ increases, the MA filter loses its ability to whiten broadband spectral features. The effect of the missing weights near the front of the filter cannot be totally compensated for by simply adding more weights to the end. Alexander has reported some of the consequences of this limitation for the case of band-limited signals in low pass noise (ref 8).

For high-SNR narrowband signals, there are no features of broad spectral extent (except for flat noise background, which can be modeled since $C_0 \neq 0$); therefore the use of this spectral estimate may be justified. Because of this possible utility, the $S_x(\omega)$ estimate for $\Delta \neq 1$ will also be studied as part of this report, and it will be referred to simply as the $S(\omega)$ estimate.

The remainder of this report will address the problem of resolution in terms of the three types of spectral estimates just described – the magnitude of H spectrum, $|H(\omega)|$; the maximum entropy spectrum, $Q(\omega)$; and the modified maximum entropy spectrum, $S(\omega)$.

EXACT SOLUTION FOR THE OPTIMUM ALE WEIGHT VECTOR

The equations defining $|H(\omega)|$, $Q(\omega)$, and $S(\omega)$ show that each of these spectral estimates is readily formed, given the converged ALE weight vector $\underset{\sim}{W}^{\star}$. Therefore, the

17. Griffiths, LJ, Rapid Measurement of Digital Instantaneous Frequency, IEEE Trans on Acoustics, Speech and Signal Processing, vol ASSP-23, p 207-222, April 1975

results of this report rely heavily on the work of Zeidler and Satorius in formulating a simplified solution of $\underset{\sim}{W}^{\star}$ for an ALE input consisting of multiple sinusoids in white noise (ref 2). The elements of the solution are here outlined.

The input signal is taken to be composed of N sinusoids of frequency ω_n and power σ_n^2 in the presence of white noise with spectral power density σ_0^2. The relative phases of the input sinusoids do not effect $\underset{\sim}{W}^{\star}$ and therefore do not form part of the problem definition.

For an L-weight ALE with bulk delay Δ, the set of optimum ALE weights $W^{\star}(k)$ is given by the solution to the following matrix equation:

$$\sum_{k=0}^{L-1} \phi_{xx}(\ell - k)\, W^{\star}(k) = \phi_{xx}(\ell + \Delta) \quad , \; 0 \leqslant \ell \leqslant L - 1 \quad . \tag{20}$$

Here $\phi_{xx}(j)$ is the signal autocorrelation function $\phi_{xx}(j) = E[X(k)X(k+j)]$. For the signal specified above, the autocorrelation function is as follows:

$$\phi_{xx}(k) = \sigma_0^2 \delta(k) + \sum_{n=1}^{n} \sigma_n^2 \cos \omega_n k \quad , \tag{21}$$

where $\delta(k)$ is the Kronecker delta function.

The solution to equation 20 (an L by L matrix system) was shown to be uniquely given by the expression

$$W^{\star}(k) = \sum_{n=1}^{2N} A_n e^{j\omega_n k} \quad , \tag{22}$$

where $\omega_{N+n} = -\omega_n$, and the coefficients A_n are given by the solution to the following 2N by 2N matrix equation:

$$A_r + \sum_{\substack{n-1 \\ n \neq r}}^{2N} \gamma_{rn} A_n = \frac{e^{j\omega_r \Delta}}{\left[L + \dfrac{2\sigma_0^2}{\sigma_r^2} \right]} \quad , r = 1, 2, \ldots, 2N \quad . \tag{23}$$

In equation 23,

$$\gamma_{rn} = \left(\frac{1}{L + \dfrac{2\sigma_0^2}{\sigma_r^2}} \right) \left(\frac{1 - e^{j(\omega_n - \omega_r)L}}{1 - e^{j(\omega_n - \omega_r)}} \right) \quad . \tag{24}$$

Since in most instances $L \gg 2N$, this solution results in a great reduction in the amount of numerical calculation required to solve for the weights. As next explained, this simplicity also facilitates an analytical investigation of the weight vector.

PROPERTIES OF THE WEIGHT VECTOR SOLUTION

Most of the work appearing later, under Results, was done by numerically solving equation 23 for a variety of signal input states. Most of the insights into the ALE's performance, however, came by analytically studying approximate solutions for the weight vector and the resulting $|H(\omega)|$, $Q(\omega)$, and $S(\omega)$ spectral estimates. Therefore, the goal of the remaining part of this section is to develop approximations to the exact equations approximations yielding mathematically tractable solutions that retain most of the salient features of the exact solution.

One approximate solution can be formulated when certain of the γ_{ij}'s are negligible (ref 2). For the case of two sinusoids it is often possible to neglect the γ_{ij}'s that couple the positive frequency components to the negative frequency components (ie, $\gamma_{13}, \gamma_{31}, \gamma_{14}, \gamma_{41}, \gamma_{23}, \gamma_{32}, \gamma_{24}, \gamma_{42} \approx 0$).

With this approximation, Zeidler, Satorius, et al (ref 2) have shown that

$$A_1 = \overline{A}_3$$

$$= \frac{1}{1 - \gamma_{12}\gamma_{21}} \left[\frac{e^{j\omega_1\Delta}}{L + \frac{2\sigma_0^2}{\sigma_1^2}} - \frac{\gamma_{12} e^{j\omega_2\Delta}}{L + \frac{2\sigma_0^2}{\sigma_2^2}} \right] \tag{25a}$$

and

$$A_2 = \overline{A}_4$$

$$= \frac{1}{1 - \gamma_{12}\gamma_{21}} \left[\frac{e^{j\omega_2\Delta}}{L + \frac{2\sigma_0^2}{\sigma_2^2}} - \frac{\gamma_{21} e^{j\omega_1\Delta}}{L + \frac{2\sigma_0^2}{\sigma_1^2}} \right] , \tag{25b}$$

where the bar denotes complex conjugation. This permits direct evaluation of $H^{\star}(\omega)$ by the following equation (derived from equations 4 and 22):

$$H^{\star}(\omega) = \sum_{n=1}^{2N} A_n e^{-j\omega} \left[\frac{1 - e^{j(\omega_n - \omega)L}}{1 - e^{j(\omega_n - \omega)}} \right] . \tag{26}$$

A further simplification is appropriate when $|\omega_1 - \omega_2|$ is small compared with ω_{AV} and when the domain of $H(\omega)$ is limited to $\omega \geq 0$. The approximation $A_3 = 0$, $A_4 = 0$ yields the following expression for $H^{\star}(\omega)$:

$$H^{\star}(\omega) = \left[A_1 \frac{1 - e^{j(\omega_1 - \omega)L}}{1 - e^{j(\omega_1 - \omega)}} + A_2 \frac{1 - e^{j(\omega_2 - \omega)L}}{1 - e^{j(\omega_2 - \omega)}} \right] e^{-j\omega} , \tag{27}$$

where A_1 and A_2 are given by equation 25.

Figures 4 and 5 show the effect of these approximations on the function $|H(\omega)|$. The solid line shows the exact solution given by equation 23; the dashed line was calculated according to equation 27. In figure 4, where $|\omega_1 - \omega_2| / \omega_{AV} = 0.9$, the approximation provides a qualitative representation of the exact function over the entire range of ω and performs very well in the region of interest ($\omega_1 \leq \omega \leq \omega_2$). In figure 5, where $|\omega_1 - \omega_2|/\omega_{AV} = 0.25$, the difference between the approximate solution (which is symmetric about ω_{AV}) and the exact value of $|H^{\star}(\omega)|$ (which is asymmetric about ω_{AV} due to interference from negative frequency terms) is more noticeable for small values of ω. Even in this case, equation 27 provides a good approximation in the region near the primary peaks.

Using equation 27 as a model for ALE response, a physical appreciation can be developed for the properties of $H^{\star}(\omega)$ and the $|H^{\star}(\omega)|$ spectral estimate.

With the definitions given in equation 25, equation 27 can be written as

$$H^{\star}(\omega) = \frac{e^{-j\omega}}{1 - \gamma_{12}\gamma_{21}} \left\{ \left(\theta_1 e^{j\omega_1 \Delta} - \theta_2 \gamma_{21} e^{j\omega_2} \right) F(\omega, L, \omega_1)\, e^{j \left[\frac{\omega_1 - \omega}{2} (L-1) \right]} \right.$$

$$\left. + \left(\theta_2 e^{j\omega_2 \Delta} - \theta_1 \gamma_{21} e^{j\omega_1 \Delta} \right) F(\omega, L, \omega_2)\, e^{j \left[\frac{\omega_2 - \omega}{2} (L-1) \right]} \right\} , \qquad (28)$$

where

$$\theta_i = \left(L + \frac{2\sigma_0^2}{\sigma_1^2} \right)^{-1} , \quad i = 1, 2 , \qquad (29)$$

and

$$F(\omega, L, \omega_1) = \frac{\sin \frac{\omega_i - \omega}{2} L}{\sin \frac{\omega_i - \omega}{2}} . \qquad (30)$$

Equation 30 results from the identity

$$\frac{1 - e^{-j\omega L}}{1 - e^{-j\omega}} = e^{-j \left(\frac{N-1}{2} \right) \omega} \frac{\sin (L/2)\omega}{\sin (1/2)\omega}$$

By factoring out exponentials and collecting terms it can be shown that equation (28) is equivalent to

$$H^{\star}(\omega) = \left\{ \frac{e^{-j\omega}\, e^{-j \left[\frac{\omega_1 - \omega}{2} (L-1) \right]}}{1 - \gamma_{12}\gamma_{21}} \right\} \left\{ \theta_1 F(\omega, \omega_1, L) \left[1 - \theta_2 F(\omega_1, \omega_2, L)\, e^{j\phi} \right] \right.$$

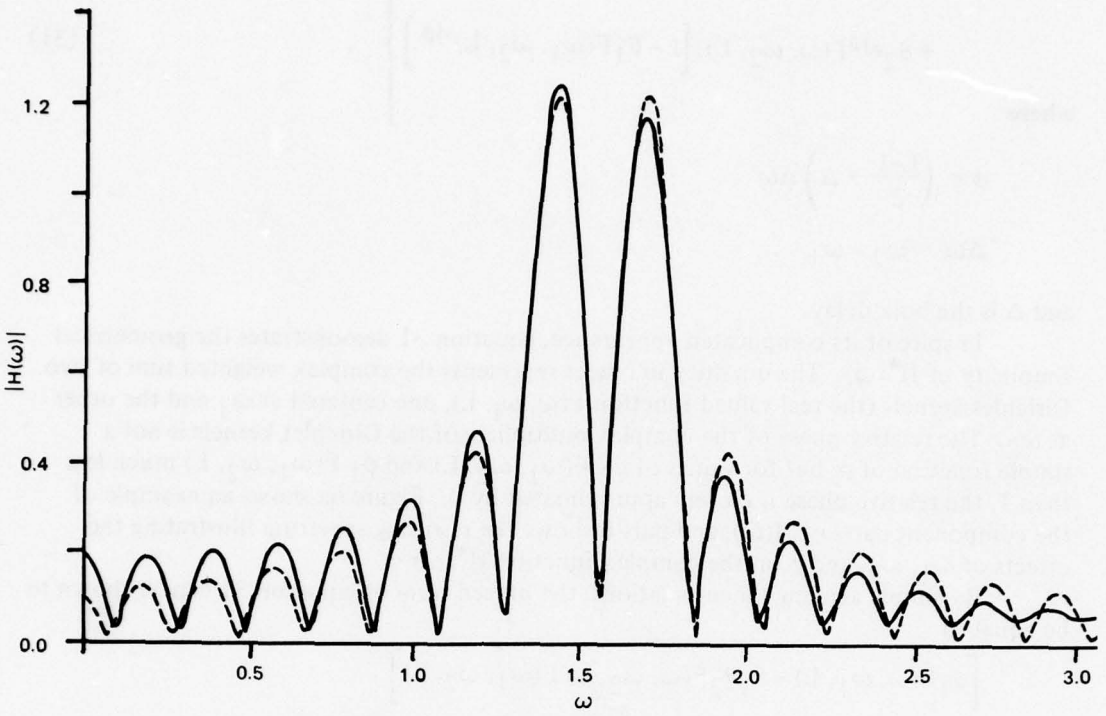

Figure 4. $|H(\omega)|$ exact (solid) and approximate (dashed) solutions for L = 32, 0 dB SNR for each sinusoid, $\omega_1 = 1.48$, $\omega_2 = 1.62$, and $\Delta = 6$.

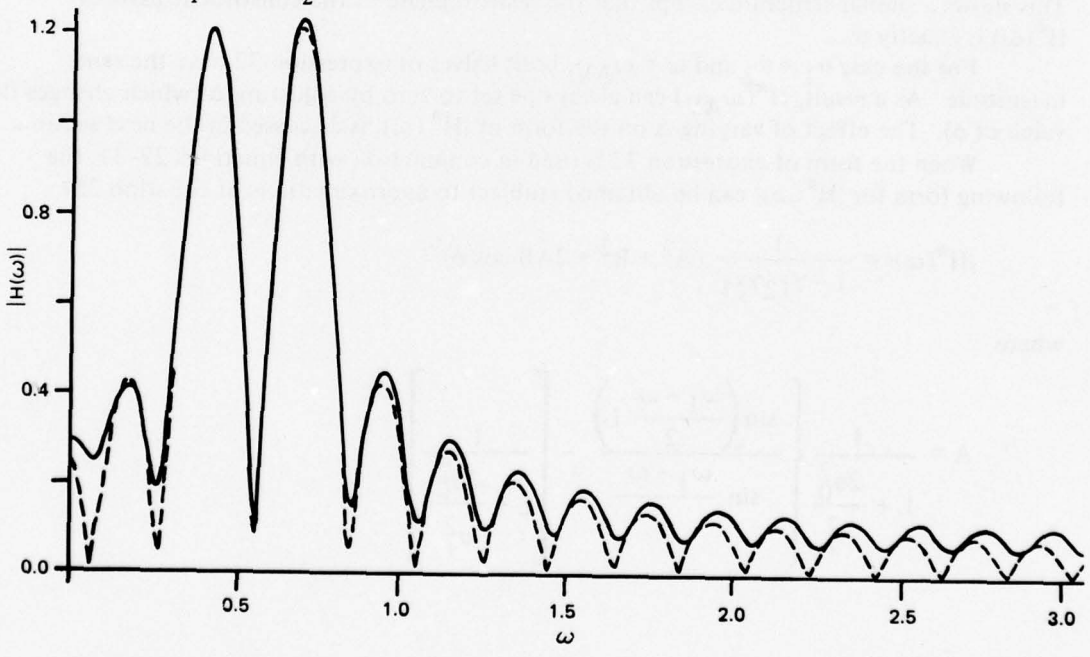

Figure 5. $|H(\omega)|$ exact (solid) and approximate (dashed) solutions for L = 32, 0 dB SNR for each sinusoid, $\omega_1 = 0.48$, $\omega_2 = 0.62$, and $\Delta = 6$.

$$+ \theta_2 e^{j\phi} F(\omega, \omega_2, L) \left[1 - \theta_1 F(\omega_1, \omega_2, L) e^{-j\phi}\right] \Bigg\} \quad , \tag{31}$$

where

$$\phi = \left(\frac{L-1}{2} + \Delta\right) \Delta\omega \quad ,$$

$$\Delta\omega = \omega_2 - \omega_1 \quad ,$$

and Δ is the bulk delay.

In spite of its complicated appearance, equation 31 demonstrates the geometrical simplicity of $H^{\star}(\omega)$. The quantity in braces represents the complex weighted sum of two Dirichlet kernels (the real-valued function $F(\omega, \omega_i, L)$, one centered at ω_1 and the other at ω_2. The relative phase of the complex multipliers of the Dirichlet kernels is not a simple function of ϕ; but for values of $\theta_2\ F(\omega_1, \omega_2, L)$ and $\phi_1\ F(\omega_1, \omega_2, L)$ much less than 1, the relative phase is closely approximated by ϕ. Figure 6a shows an example of the component parts of $H(\omega)$, and part b shows the resulting spectrum illustrating the effects of ω_1, ω_2, and ϕ on the complex function $H^{\star}(\omega)$.

By simple algebraic manipulations, the braced term of equation 31 can be shown to be equal to

$$\left[\theta_1 F(\omega, \omega_1, L) - \theta_1\theta_2 F(\omega, \omega_2, L)\ F(\omega_1, \omega_2, L)\right]$$

$$+ \left[\theta_2 F(\omega_2, \omega_1, L) - \phi_1\phi_2 F(\omega_2, \omega_1, L) F(\omega, \omega_1, L)\right] e^{j\phi} \quad . \tag{32}$$

This shows a similar structure except that the relative phase of the constituent parts of $H^{\star}(\omega)$ is exactly ϕ.

For the case $\theta_1 = \theta_2$ and $\omega = \omega_{AV}$, both halves of expression 32 have the same magnitude. As a result, $H^{\star}(\omega_{AV})$ can always be set to zero by adjusting Δ (which changes the value of ϕ). The effect of varying Δ on the form of $|H^{\star}(\omega)|$ is discussed in the next section.

When the form of expression 32 is used in conjunction with equations 29–31, the following form for $|H^{\star}(\omega)|$ can be obtained (subject to approximations of equation 25).

$$|H^{\star}(\omega)| = \frac{1}{1 - \gamma_{12}\gamma_{21}} \left(A^2 + B^2 + 2AB \cos\phi\right)^{1/2}$$

where

$$A = \frac{1}{L + \dfrac{2\sigma_0^2}{\sigma_1^2}} \left\{ \frac{\sin\left(\dfrac{\omega_1 - \omega}{2} L\right)}{\sin\dfrac{\omega_1 - \omega}{2}} - \left[\frac{1}{L + \dfrac{2\sigma_0^2}{\sigma_1^2}} \right] \right.$$

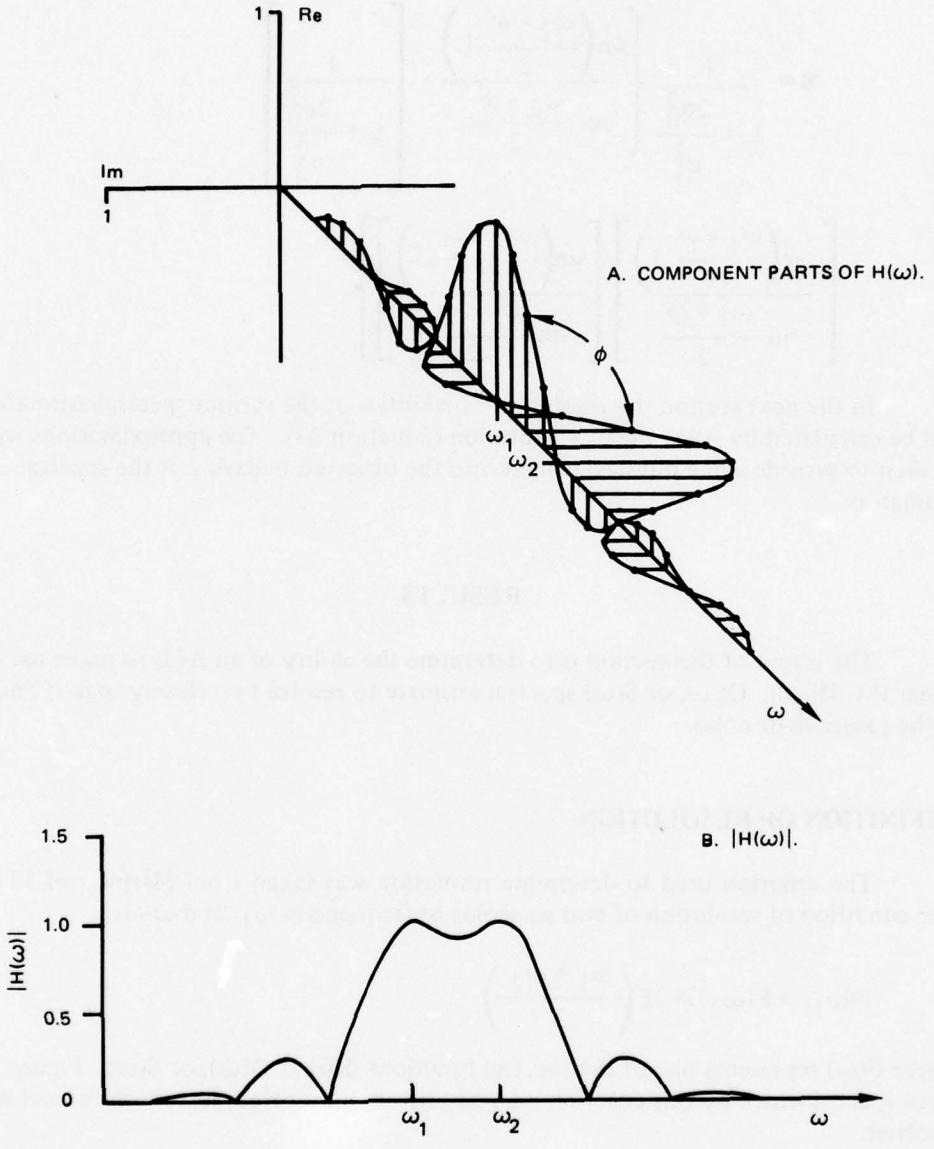

Figure 6. For two sinusoids, $H(\omega)$ is composed of two Dirichlet kernels centered at ω_1 and ω_2 and separated by ϕ in complex phase as shown in part A. The resulting $|H(\omega)|$ spectrum is shown in B.

$$\left[\frac{\sin\left(\frac{\omega_2-\omega}{2}L\right)}{\sin\frac{\omega_2-\omega}{2}}\right]\left[\frac{\sin\left(\frac{\omega_2-\omega_1}{2}L\right)}{\sin\frac{\omega_2-\omega_1}{2}}\right]\Bigg\}$$

$$B = \frac{1}{L+\frac{2\sigma_0^2}{\sigma_1^2}}\left\{\frac{\sin\left(\frac{\omega_2-\omega}{2}L\right)}{\sin\frac{\omega_2-\omega}{2}} - \left[\frac{1}{L+\frac{2\sigma_0^2}{\sigma_2^2}}\right]\right.$$

$$\left[\frac{\sin\left(\frac{\omega_1-\omega}{2}L\right)}{\sin\frac{\omega_1-\omega}{2}}\right]\left[\frac{\sin\left(\frac{\omega_2-\omega_1}{2}L\right)}{\sin\frac{\omega_2-\omega_1}{2}}\right]\Bigg\} \quad . \tag{33}$$

In the next section the resolution capabilities of the various spectral estimators will be calculated by using the exact solution (equation 23). The approximations will be used to provide some physical insight into the observed behavior of the spectral estimators.

RESULTS

The intent of this section is to determine the ability of an ALE to make use of either the $|H(\omega)|$, $Q(\omega)$, or $S(\omega)$ spectral estimate to resolve two closely spaced lines in the presence of noise.

DEFINITION OF RESOLUTION

The criterion used to determine resolution was taken from Marple (ref 11). The condition of resolution of two sinusoids of frequencies ω_1 and ω_2 is

$$F(\omega_1) + F(\omega_2) \geq 2F\left(\frac{\omega_1+\omega_2}{2}\right) , \tag{34}$$

where $F(\omega)$ represents one of the spectral functions $|H(\omega)|$, $Q(\omega)$, or $S(\omega)$. Figure 7 shows three spectra which by this criterion are respectively unresolved, just resolved, and well-resolved.

The separation of the two spectral tones is expressed as follows:

$$R_M = L\Delta\omega\Delta t \quad , \tag{35}$$

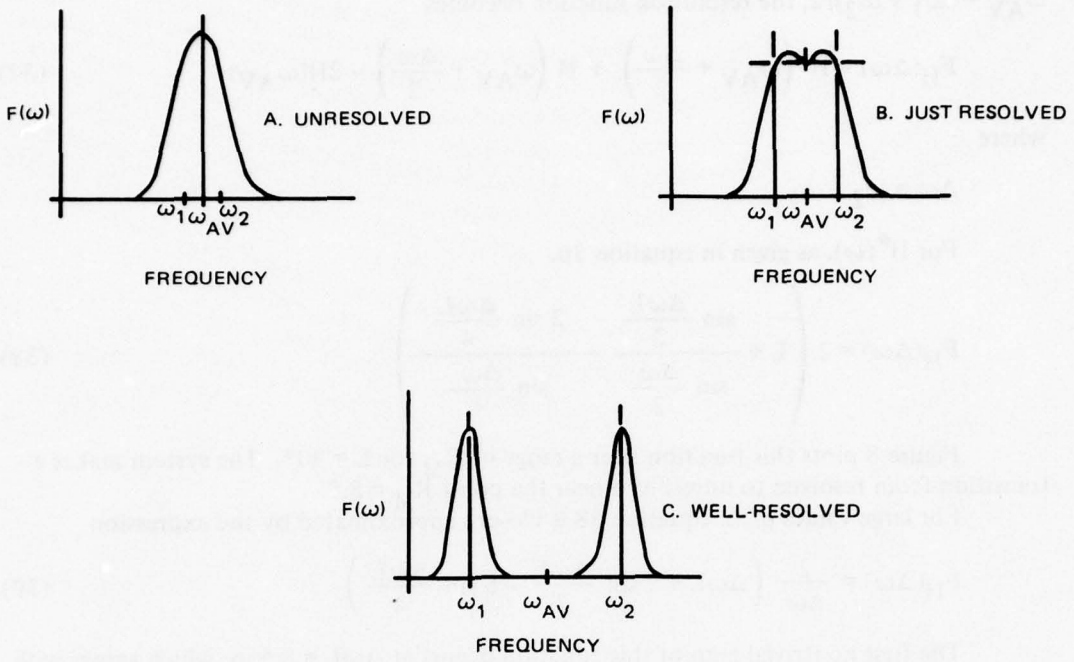

Figure 7. Spectra which by Marple's criterion are unresolved, just resolved, and well-resolved.

where L is the number of ALE weights, $\Delta\omega$ is the separation of the two tones in radian frequency, and Δt is the sampling time ($\Delta t = 1$ for all calculations herein; therefore $R_M = L\Delta\omega$). Marple refers to R_M as the modified normalized resolution (ref 11). In this report R_M is simply called the resolution.

This concept of resolution is demonstrated by using as an example an $|H(\omega)|$ which is simply the sum of two Dirichlet kernels of the same magnitude:

$$H^{\star}(\omega) = \frac{\sin\left(\frac{\omega_1 - \omega}{2} L\right)}{\sin\frac{\omega_1 - \omega}{2}} + \frac{\sin\left(\frac{\omega_2 - \omega}{2} L\right)}{\sin\frac{\omega_2 - \omega}{2}} \quad . \tag{36}$$

This criterion for resolution can be expressed in terms of a single real-valued function

$$F_H(\omega_1, \omega_2) = H(\omega_1) + H(\omega_2) - 2H\left(\frac{\omega_1 + \omega_2}{2}\right)$$
$$> 0.$$

The limit of resolution can then be determined by decreasing $|\omega_1 - \omega_2|$ until $F_H(\omega_1, \omega_2) = 0$.

When the two tones uniformly approach ω_{AV}, their average frequency, where $\omega_{AV} = (\omega_1 + \omega_2)/2$, the resolution function becomes

$$F_H(\Delta\omega) = H\left(\omega_{AV} + \frac{\Delta\omega}{2}\right) + H\left(\omega_{AV} + \frac{\Delta\omega}{2}\right) - 2H(\omega_{AV}) \quad , \tag{37}$$

where

$$\Delta\omega = \omega_2 - \omega_1 \quad .$$

For $H^{\star}(\omega)$, as given in equation 36,

$$F_H(\Delta\omega) = 2\left(L + \frac{\sin\frac{\Delta\omega L}{2}}{\sin\frac{\Delta\omega}{2}} - \frac{2\sin\frac{\Delta\omega L}{4}}{\sin\frac{\Delta\omega}{4}}\right) \quad . \tag{38}$$

Figure 8 plots this function over a range of R_M for L = 30*. The system makes a transition from resolved to unresolved near the point $R_M = 8.5$.

For large values of L, equation 38 is closely approximated by the expression

$$F_H(\Delta\omega) = \frac{2}{\Delta\omega}\left(\Delta\omega L + 2\sin\frac{\Delta\omega L}{2} - 8\sin\frac{\Delta\omega L}{4}\right) \quad . \tag{39}$$

The first nontrivial zero of this equation occurs at $\Delta\omega L = 8.556$, which agrees with the transition point shown in figure 8. It is noted that as measured by R_M, the limit of resolution is independent of L.

This example demonstrates the basic approach used here. A real-valued function is formed from the values of $|H^{\star}(\omega)|$, $Q(\omega)$, or $S(\omega)$ at frequencies ω_1, ω_2, and ω_{AV} and is tested to determine whether it is positive or negative (ie, respectively resolved or unresolved). The limit of resolution is determined by fixing ω_{AV}, then varying $\Delta\omega$ until $F(\Delta\omega) = 0$.

REGIONS VS LIMITS OF RESOLUTION

The concept of a limit of resolution implies the existence of a single critical frequency difference $\Delta\omega$ which separates resolved and unresolved spectra. Figure 8 is consistent with this relationship, as shown by the single change in the sign of $F_H(\Delta\omega)$ at $R_M = 8.556$.

Figures 9 and 10 demonstrate some of the complications that arise when Δ rather than ϕ is fixed. Figure 9 shows $F_H(\Delta\omega)$ for the identical signal and ALE used in figure 8 except that Δ is set to 1. Although this change results in a definite limit of resolution (ie, one zero crossing), the monotonic behavior of $F_H(\Delta\omega)$ in the resolved region is no longer present. The dotted line shows the $\phi = 0$ case (ie, figure 8), for comparison.

In figure 10, $\Delta = 100$. Again, the $\phi = 0$ case is shown dotted for comparison. In this case the ALE does not have a definite limit of resolution, but alternately traverses resolved and unresolved regions as the frequency separation is decreased. The effect as seen in the individual spectra is shown in figures 11-13. For an ALE with L = 15 and $\Delta = 5$ the

*Numerical values of $F_H(\Delta\omega)$ were calculated from equation 33 for $\sigma_0/\sigma_1 = 2$, $\sigma_0/\sigma_2 = 2$.

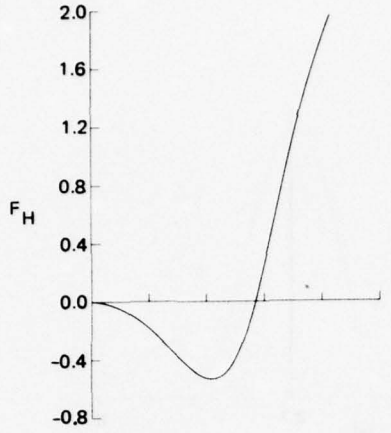

Figure 8. F_H vs R_M for L = 30, ϕ held fixed at zero.

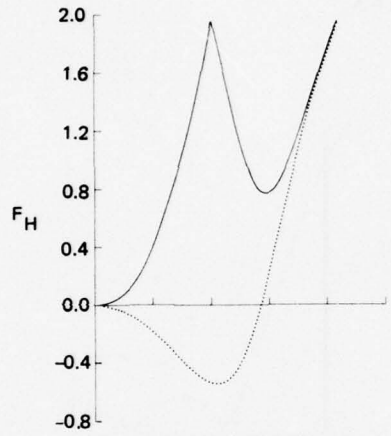

Figure 9. F_H vs R_M for L = 30 and $\sigma_1/\sigma_0 = 2$, $\sigma_2/\sigma_0 = 2$, $\Delta = 1$. Dotted curve is the $\phi = 0$ line (as in fig 8).

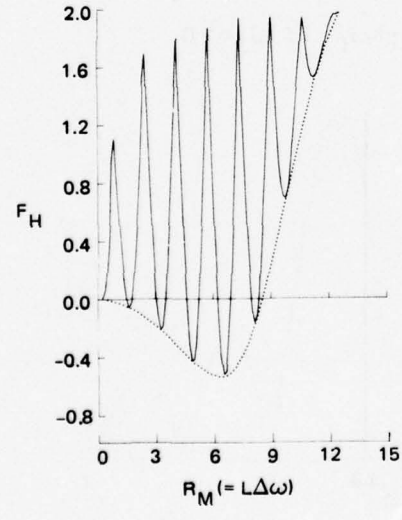

Figure 10. F_H vs R_M for L = 30 and $\sigma_1/\sigma_0 = 2$, $\sigma_2/\sigma_0 = 2$, $\Delta = 100$. Dotted curve is the $\phi = 0$ line (as in fig 8).

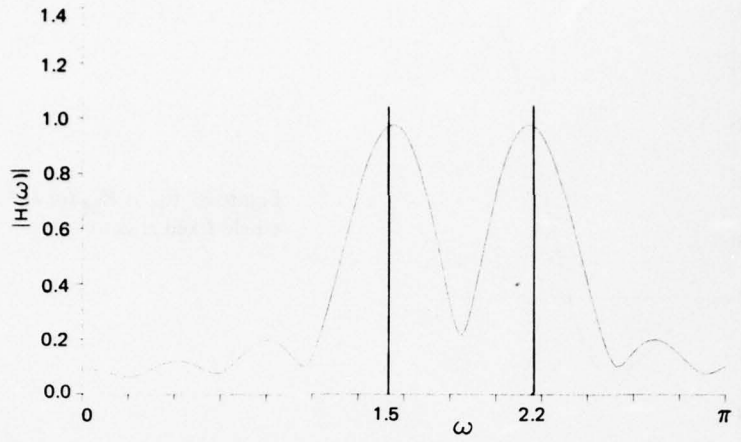

Figure 11. $|H(\omega)|$ vs ω for two tones, $\omega_1 = 1.5$, $\omega_2 = 2.2$, $\sigma_1/\sigma_0 = 2$, $\sigma_2/\sigma_0 = 2$, from ALE with L = 15 and $\Delta = 5$.

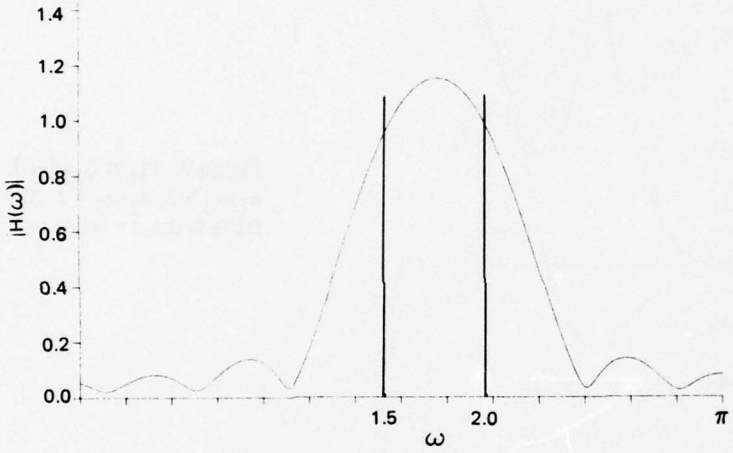

Figure 12. Same as fig 11 except $\omega_1 = 1.5$, $\omega_2 = 2.0$.

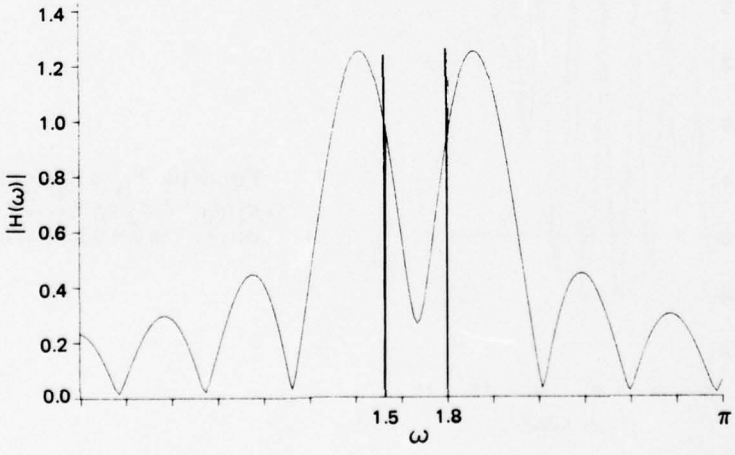

Figure 13. Same as fig 11 except $\omega_1 = 1.5$, $\omega_2 = 1.8$.

spectra are resolved, unresolved, and resolved respectively for R_M equal to 10.50, 7.50 and 4.50. While figure 13 shows a resolved spectrum, the peaks in $|H(\omega)|$ are seen to be far from the indicated frequencies of the input sinusoids.

Figures 14–17 show the phenomenon of multiple regions of resolution in a different form. In these figures F_H was calculated for a matrix of conditions representing different values of R_M and L. Locations on the grid where the spectrum was resolved are marked with a U. These figures represent solutions to the approximate expressions for ALE response as given in equation 27. For small values of L, the coupling between the tone frequencies becomes significant and can result in values of R_M exceeding 8.56, a limit which was calculated under the assumption of zero coupling between positive and negative frequencies. Thus for moderate and large values of L ($L > 10$), the previously calculated limit of R_M is correct.

As shown in these figures, increasing Δ results in the appearance and growth of disconnected regions of unresolved spectra. Figure 18 for example, shows similar regions of resolution that were found by using the modified maximum entropy spectral estimate $S(\omega)$ with $\Delta = 30$.

The "ALE limit of spectral resolution" concept must be enlarged to accommodate the observed property of regions of spectral resolution.

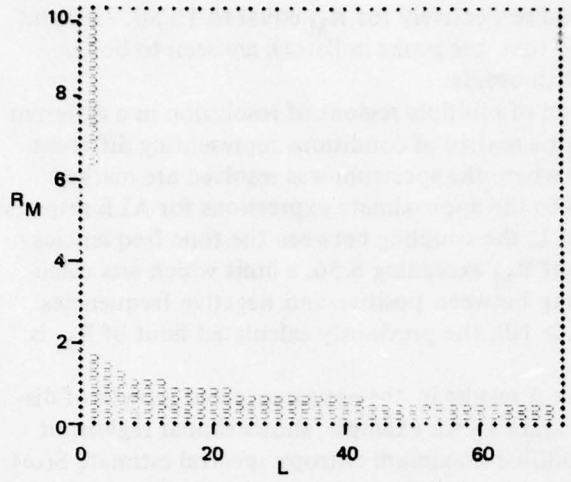

Figure 14. Regions where Marple's criterion judged the ALE $|H(\omega)|$ spectrum to be unresolved, for $\sigma_1/\sigma_0 = 2$, $\sigma_2/\sigma_0 = 2$, $\Delta = 1$.

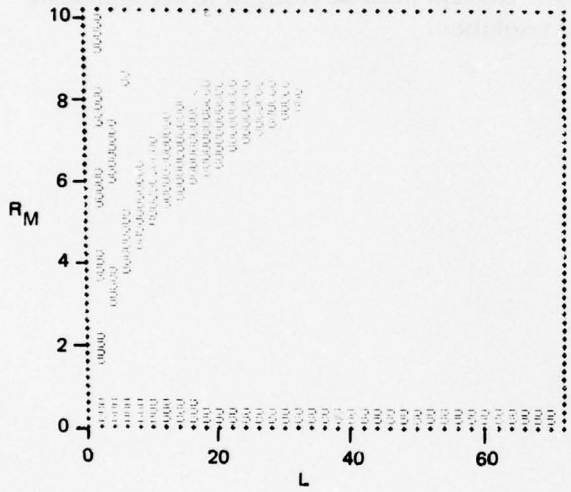

Figure 15. Same as fig 14 except $\Delta = 6$.

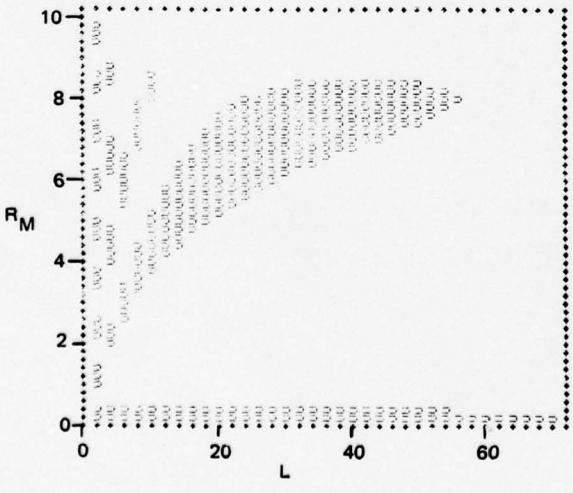

Figure 16. Same as fig 14 except $\Delta = 10$.

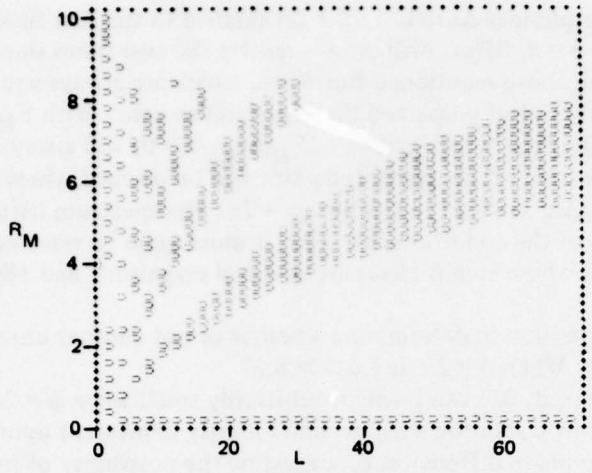

Figure 17. Same as fig 14 except $\Delta = 30$.

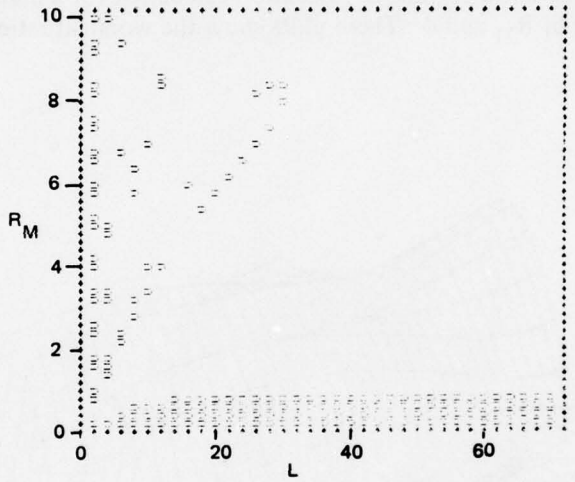

Figure 18. Unresolved regions for $S(\omega)$ derived from ALE weights, for $\sigma_1/\sigma_0 = 2$, $\sigma_2/\sigma_0 = 2$, $\Delta = 30$. This calculation was made by using equation 23 with $\omega_{AV} = 1.57$.

ORIGIN OF MULTIPLE REGIONS OF RESOLUTION

The origin of multiple regions of resolution can be understood in terms of equation 32 and figure 6. In this representation, $H^{\star}(\omega)$ is the complex sum of two functions with approximate Dirichlet kernels. The phase difference between these functions (as in figure 6) is given by the expression, $\phi = \Delta\omega[(L-1)/2 + \Delta]$. When $\Delta\omega = 0$, the two kernels coincide and only one peak is visible in $|H^{\star}(\omega)|$. As $\Delta\omega$ increases, the sum inside the brackets of equation 32 is composed of one stationary function positioned at ω_1 and one

positioned at ω_2 whose phase is $\Delta\omega[(L-1)/2 + \Delta]$ relative to the first function. When $\Delta\omega$ has increased such that $\phi = \pi$, $|H(\omega)|$ will always resolve the two tones since the contributions to $H^{\star}(\omega)$ from the above-mentioned functions, which are always equal in magnitude at ω_{AV}, are then exactly out of phase and therefore add to zero. With $F_H(\omega_{AV}) = 0$, the criterion of resolution (ie, $F_H(\omega_1) + F_H(\omega_2) - 2F_H(\omega_{AV}) > 0$) will always be satisfied since $F_H(\omega) > 0$. As $\Delta\omega$ continues to increase, the point will be reached where $\phi = 2\pi$. As figure 8 shows, unless $L\Delta\omega > 8.5$ at that point ($\phi = 2\pi$), the spectrum $|H(\omega)|$ will again be unresolved. Regardless of the condition at $\phi = 2\pi$, it must again be resolved at $\phi = 3\pi$, 5π, etc, since the two terms whose sum is $H(\omega)$ are of equal magnitude and 180° out of phase at ω_{AV}.

An important question in determining whether or not another unresolved region will result after $\phi = \pi$ is this: When $\phi = 2\pi$, is $L\Delta\omega > 8.5$?

As already discussed, $\Delta\omega$ can be made arbitrarily small when $\phi = 2\pi$, 4π, etc by increasing Δ. The state of resolution then becomes jointly dependent upon the frequency separation, $\Delta\omega$, and the phase difference, ϕ, suggesting the possibility of improving resolution by selectively adjusting the ALE bulk delay, Δ. Figure 19 shows a surface generated from a series of $|H(\omega)|$ spectra; the input signal is the same for all the spectra. The spectrum is seen to change from unresolved to resolved as the bulk delay, Δ, is changed.

Figures 20 and 21 show regions of resolution calculated for a matrix of cases representing different values of R_M and ϕ. These plots show the worst situation for resolution

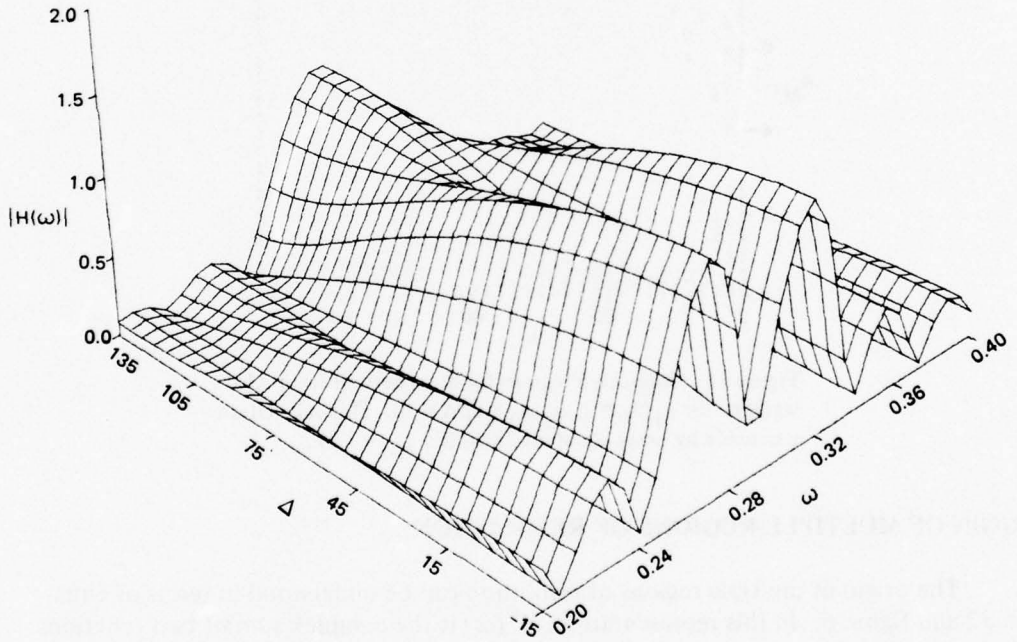

Figure 19. Surface composed of $|H(\omega)|$ spectra determined from the same input signal and ALE filter length but for different values of Δ. For this case $L = 30$, $\omega_1 = 0.28$, $\omega_2 = 0.30$, $\sigma_1/\sigma_0 = 2$, and $\sigma_2/\sigma_0 = 2$.

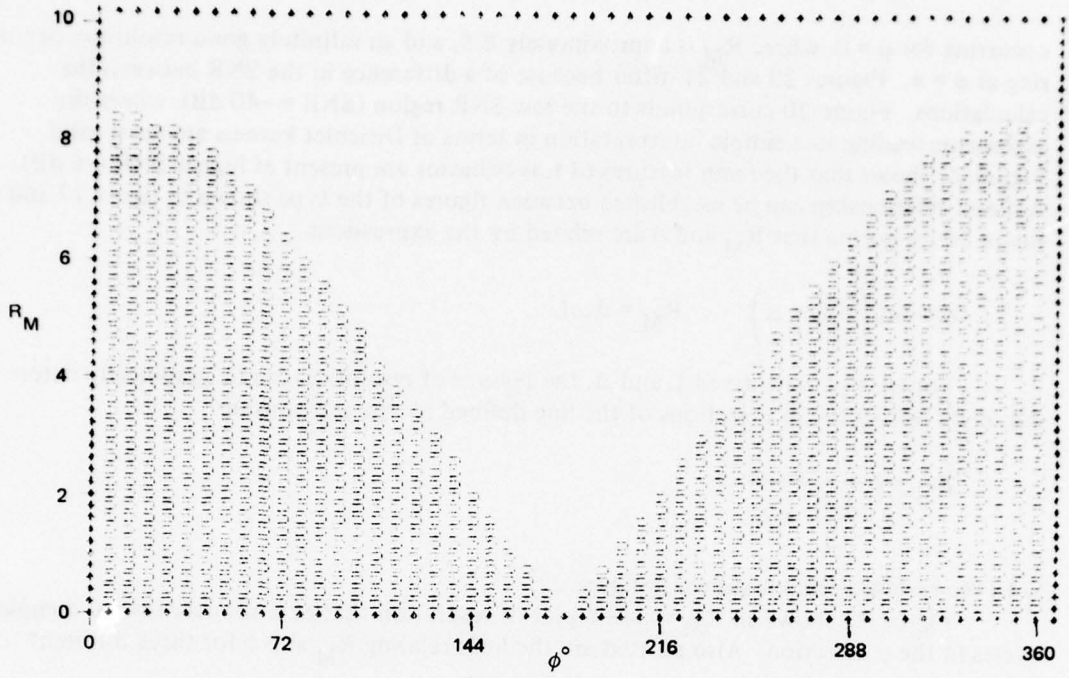

Figure 20. Regions of resolution for $|H(\omega)|$ as a function of ϕ and R_M for L = 40 and a -40 dB SNR for each sinusoid ($\sigma_i/\sigma_o = 0.01$).

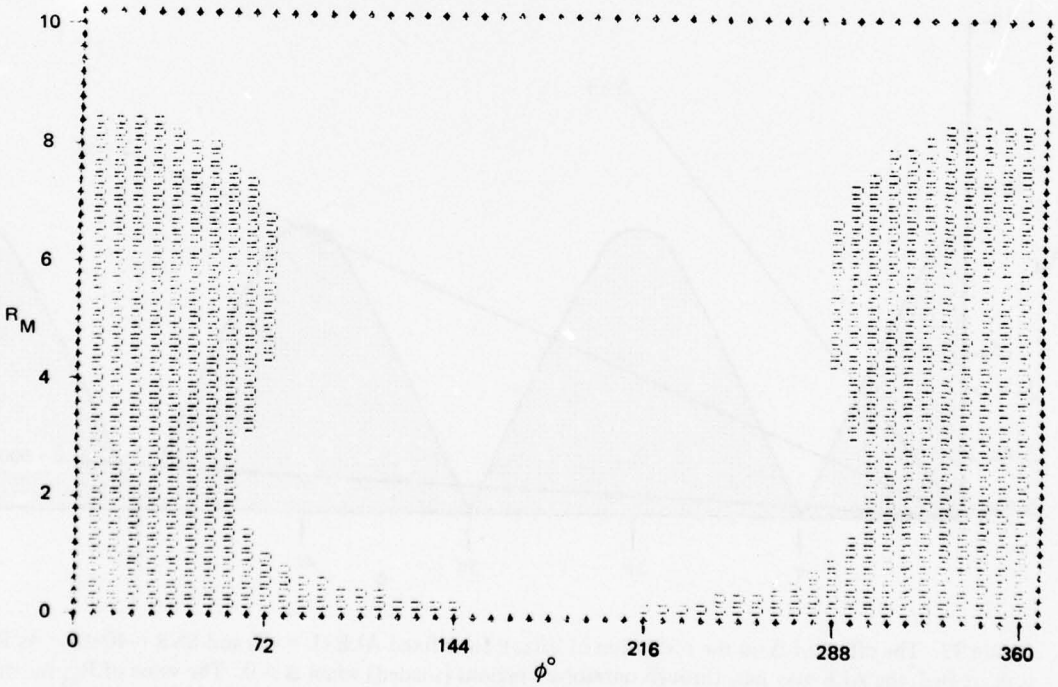

Figure 21. Regions of resolution for $|H(\omega)|$ as a function of ϕ and R_M for L = 40 and a -6 dB SNR for each sinusoid ($\sigma_i/\sigma_o = 2$).

occurring for $\phi = 0$, where R_M is approximately 8.5, and an infinitely good resolution occurring at $\phi = \pi$. Figures 20 and 21 differ because of a difference in the SNR between the calculations. Figure 20 corresponds to the low SNR region (SNR = -40 dB), where the arguments leading to a simple interpretation in terms of Dirichlet kernels are most valid. Figure 21 shows that the main features of this behavior are present at higher SNR (-6 dB). A direct relationship can be established between figures of the type shown in figure 17 and figure 20 by noting that R_M and ϕ are related by the expressions

$$\phi = \Delta\omega\left(\frac{L-1}{2} + \Delta\right) \quad , \quad R_M = \Delta\omega L \quad .$$

For an ALE with fixed L and Δ, the regions of resolution can be graphically determined by noting the intersections of the line defined by the relationship

$$R_M = \phi \frac{L}{\frac{L-1}{2} + \Delta}$$

with the resolved regions shown in figure 22.

Figure 22 shows an R_M versus ϕ plot of resolution that extends over several complete cycles in the ϕ direction. Also plotted are the lines relating R_M and ϕ for three different

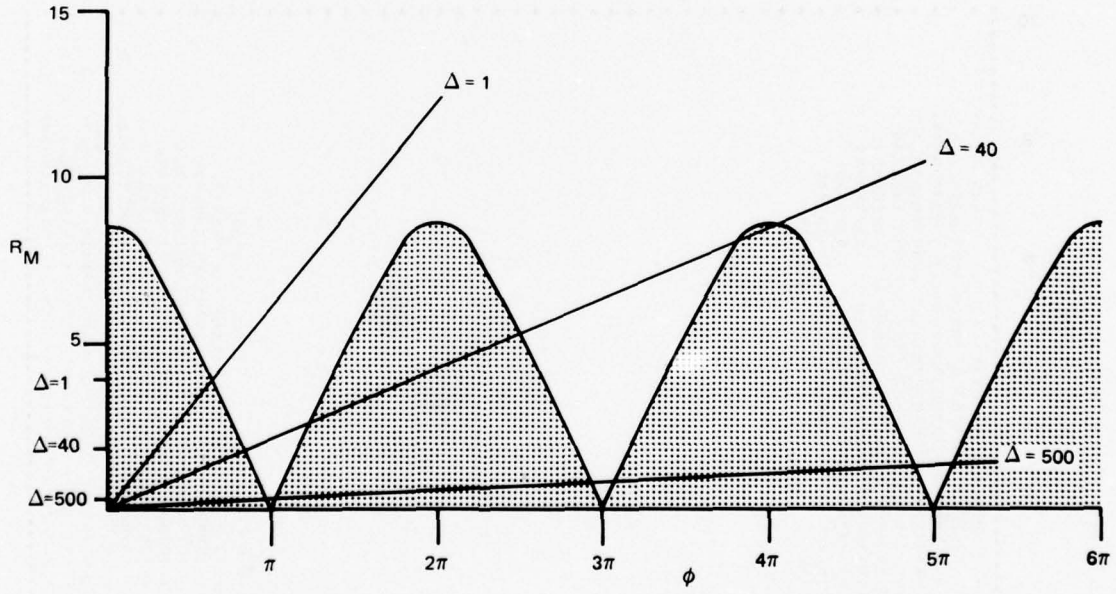

Figure 22. The effect of Δ on the resolution of $|H(\omega)|$ for a fixed ALE (L = 40) and SNR (-40 dB). As R_M is decreased, the ALE may pass through unresolved regions (shaded) when $\Delta > 0$. The value of R_M for the last resolved-unresolved transition is noted on the abscissa for several values of Δ.

values of Δ. This figure shows several interesting features of ALE resolution. First, there is only one transition between a resolved and an unresolved region for $\Delta = 1$.* In this case the concept of a limit of resolution is valid. Second, the lowest transition between resolved and unresolved occurs at a smaller value of R_M as Δ is increased. But this also results in the appearance of separate unresolved regions at larger R_M, as shown for $\Delta = 40$. Finally, the region of resolution also becomes arbitrarily small even though Δ can be adjusted to resolve lines with arbitrarily small R_M (as suggested by the $\Delta = 500$ line).

This technique of analysis relies only on the approximations needed to produce equations 25 and 27 (ie, decoupling positive-negative frequency interactions). The isolation of all Δ effects to the quantity ϕ is also correct under this approximation. The result is not completely general, since a new R_M, ϕ resolution map (fig 12, 13) must be created for each value of SNR and filter length, L.

CALCULATION OF ALE RESOLUTION

The ability of the various spectral functions, $|H(\omega)|$, $Q(\omega)$, and $S(\omega)$, to resolve two sinusoids in the presence of noise was evaluated for a variety of SNRs.

The evaluation was made by solving the exact equation for the ALE weights, forming the appropriate $F(\Delta\omega)$ function (as in equation 39) and then solving for its root. This approach is most meaningful for the case $\Delta = 1$, where there is only one nonzero root.

Since the exact solution includes contributions from negative frequencies, the resulting determination of R_M will depend on ω_{AV} as well as $\Delta\omega$. The effect of these negative frequencies is shown in figures 23 and 24. Figure 23 shows resolutions determined by solving the exact equation, 23, and from equation 27, which neglects negative-frequency components. The resolution was calculated for the case of $\phi = 0$ (Δ continuously changing with $\Delta\omega$ such that $\phi = 0$) and for $\Delta = 1$. The mean of the exact solution closely corresponds to the approximate solution in both cases. Figure 24 shows the effect of changing the center frequency of the two sinusoids. The change affects the plots of resolution R_M versus filter length L in the frequency of oscillation but not in the mean.

Figures 25–29 show the limit of resolution for $\Delta = 1$. Plotted are limiting values of resolution for $|H(\omega)|$ and $Q(\omega)$ (for $\Delta = 1$, $Q(\omega) = S(\omega)$), calculated at even values of L from 10 to 80. For these cases the $|H(\omega)|$ shows slight improvement over $Q(\omega)$, while both are significantly better than the $\phi = 0$ (worst case) value.

Figures 30–32 examine the relative resolutions of $|H(\omega)|$, $S(\omega)$, and $Q(\omega)$ for the case where $|H(\omega)|$ and $S(\omega)$ have Δ greater than 1. These figures are presented in the format of figure 14 to display the occurence of multiple regions of resolution. The $|H(\omega)|$ gives the lowest R_M for resolution but has large unresolved regions at higher values of R_M. $S(\omega)$ gives the next lower R_M for resolution. $S(\omega)$ experiences the same problem with multiple regions of resolution as $|H(\omega)|$, but this ceases to be a problem as L is increased. Finally, $Q(\omega)$ gives the poorest resolution but avoids the problem of multiple regions of resolution.

The selection of a spectral function to determine resolution is influenced by several factors. If very little is known about the signal (neither SNR nor $\Delta\omega$), then either $|H(\omega)|$ with $\Delta = 1$ or $Q(\omega)$ should be used to avoid possible error caused by the signal's being on

---

*All these figures were calculated for $L > 10$. At lower values of L the results may change slightly due to interference of positive and negative components in the weight vector solution.

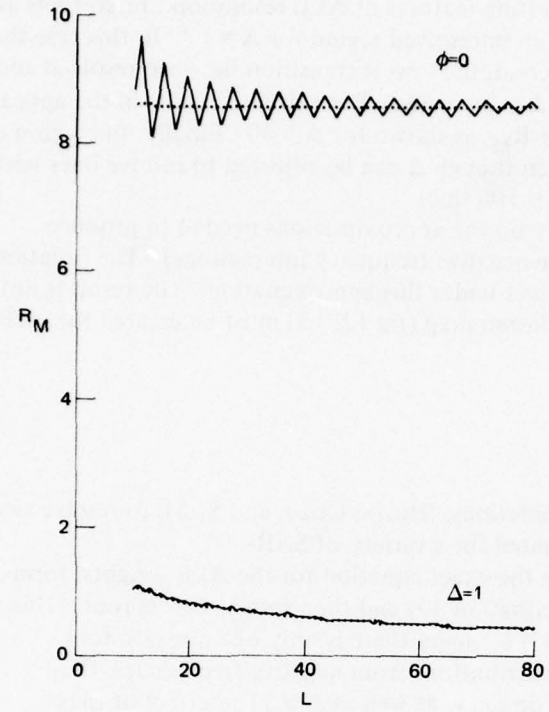

Figure 23. Limits of resolution for $|H(\omega)|$ determined by solving the exact equation, 23 (solid), and the approximate equation, 27 (dashed). For these plots $\sigma_i/\sigma_o = 2$, $\omega_{center} = 1.57$, $\Delta = 1$.

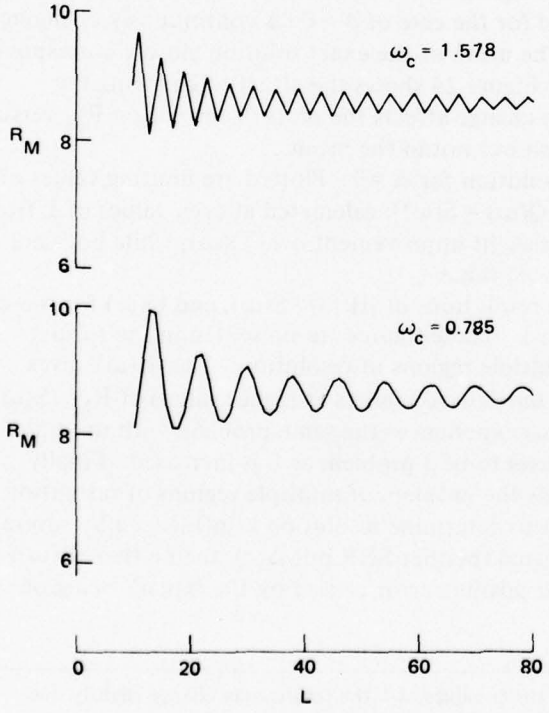

Figure 24. Limits of resolution for $|H(\omega)|$ calculated for $\omega_c = 0.785$ and 1.578. For this plot $\sigma_i/\sigma_o = 2$, $\Delta = 1$.

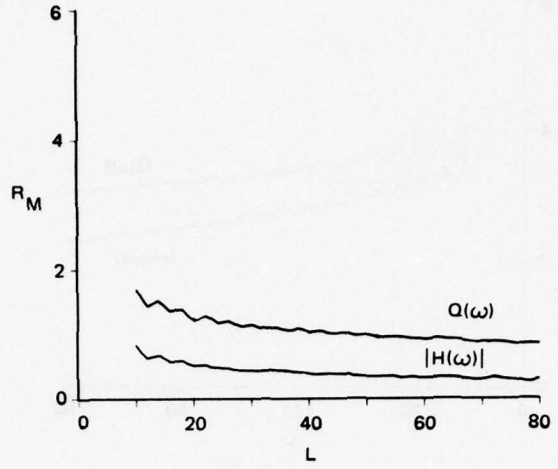

Figure 25. Limits of resolution for $|H(\omega)|$ and $Q(\omega)$ for a 10 dB signal ($\sigma_i/\sigma_o = 3.16$) with $\Delta = 1$ and $\omega_{center} = 0.785$. Solutions from exact equations.

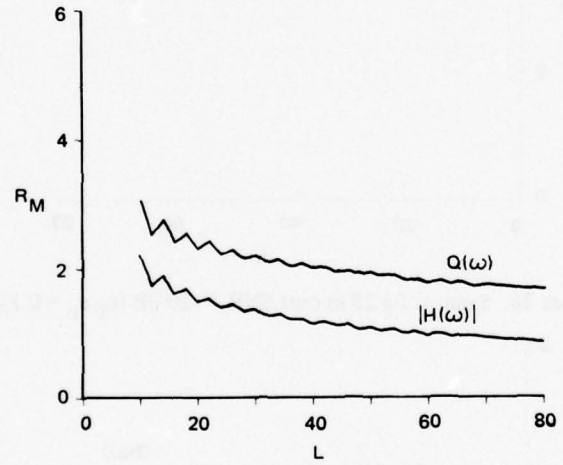

Figure 26. Same as fig 25 except SNR = 0 dB ($\sigma_i/\sigma_o = 1$).

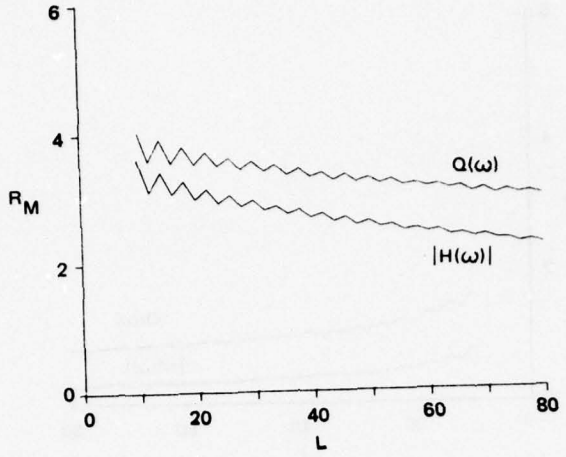

Figure 27. Same as fig 25 except SNR = 10 dB ($\sigma_i/\sigma_o = 0.32$).

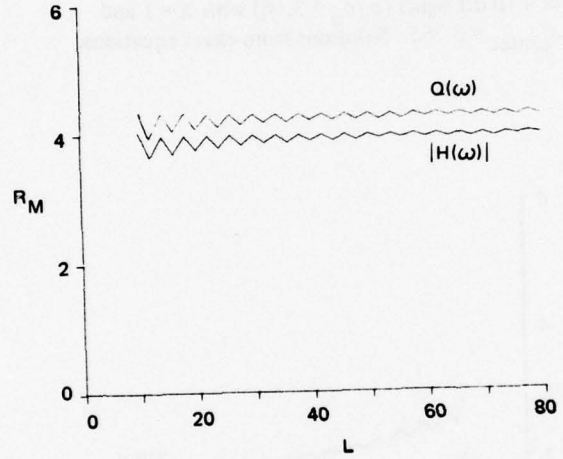

Figure 28. Same as fig 25 except SNR = -20 dB ($\sigma_i/\sigma_o = 0.1$).

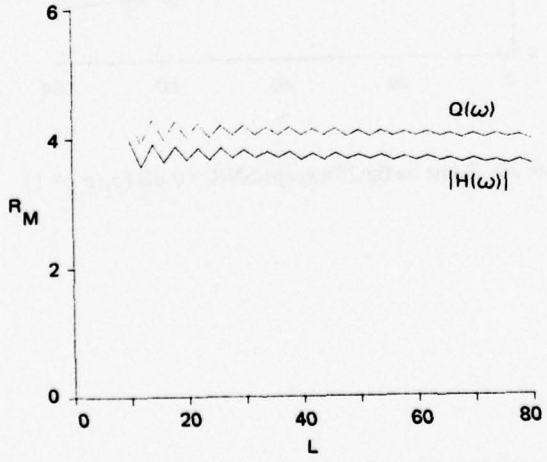

Figure 29. Same as fig 25 except SNR = -40 dB ($\sigma_i/\sigma_o = 0.01$).

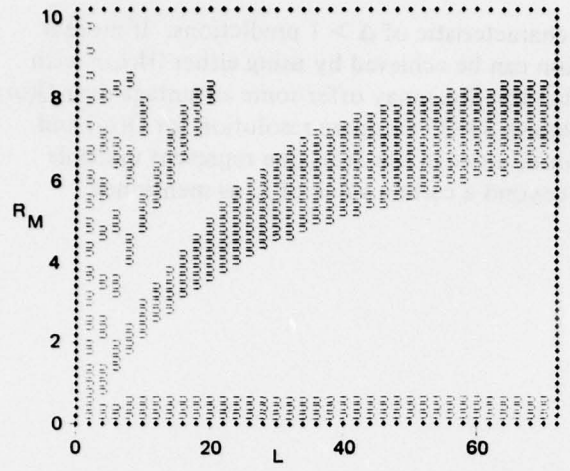

Figure 30. Resolved and unresolved regions of the $|H(\omega)|$, Δ = 20 ALE spectral estimate for SNR = 0 dB ($\sigma_i/\sigma_0 = 1$).

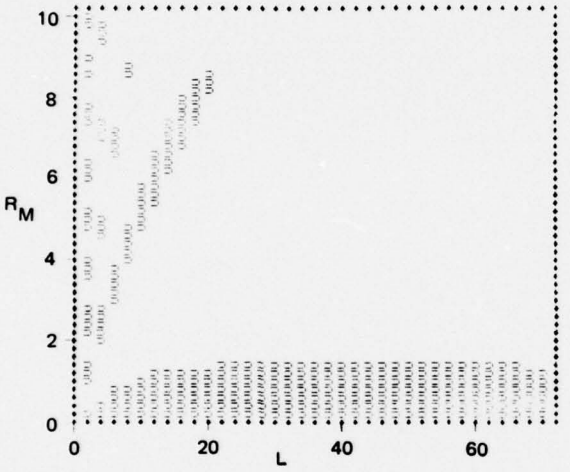

Figure 31. Same as fig 30 except plot refers to $S(\omega)$, Δ = 20 ALE spectral estimate.

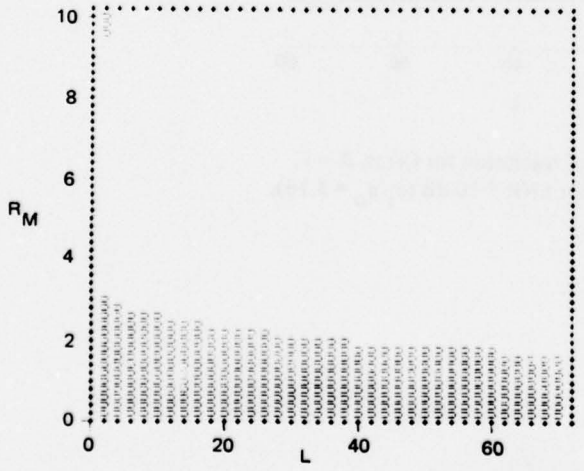

Figure 32. Same as fig 30 except plot refers to $Q(\omega)$ ALE spectral estimate.

one of the higher-level unresolved regions characteristic of $\Delta > 1$ predictions. If more is known about the signal, improved resolution can be achieved by using either $|H(\omega)|$ with $\Delta > 1$ or $S(\omega)$. Figures 30 and 31 show that the $S(\omega)$ may offer some advantage over $Q(\omega)$ when the number of weights is limited. Figures 33–35 compare resolution for $Q(\omega)$ and $S(\omega)$ ($\Delta = 20$) for several SNRs. The discontinuities in the $S(\omega)$ line represent multiple unresolved regions, a problem that ceases beyond a certain value of L, as mentioned previously.

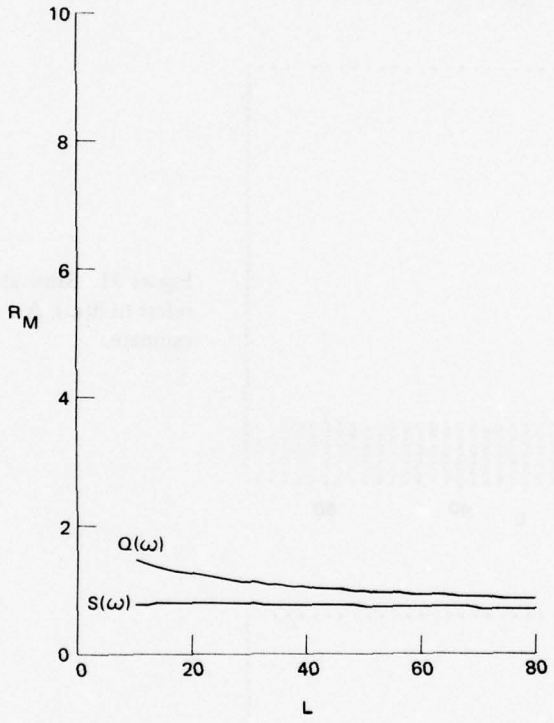

Figure 33. Limits of resolution for $Q(\omega)$, $\Delta = 1$, and $S(\omega)$, $\Delta = 20$, for SNR = 10 dB ($\sigma_i/\sigma_o = 3.16$), $\omega_{center} = 1.57$.

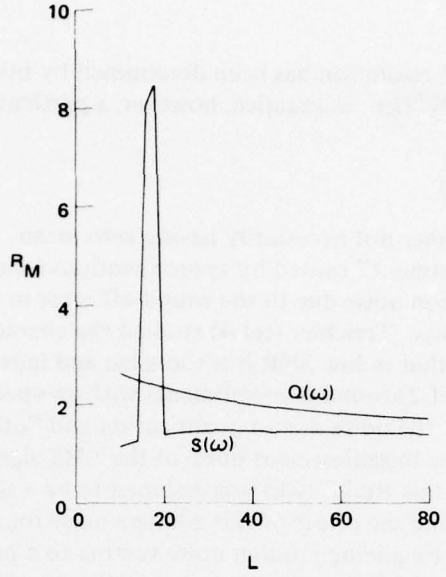

Figure 34. Same as fig 33 except SNR = 0 dB ($\sigma_i/\sigma_o = 1$).

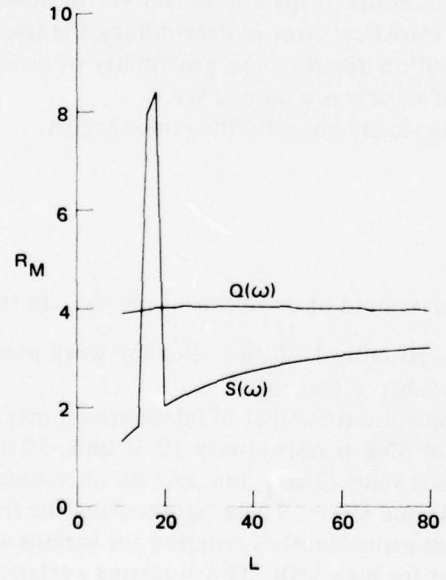

Figure 35. Same as fig 33 except SNR = -20 dB ($\sigma_i/\sigma_o = 0.1$).

ALE RESOLUTION WHEN THE WEIGHT VECTOR CONTAINS NOISE

Until this point ALE resolution has been determined by using the exact values for the optimum weight vector $W^{\star}(k)$. In practice, however, a particular measurement of the weight vector has the form

$$W(k) = W^{\star}(k) + N(k) \quad ,$$

where N(k) is a random number not necessarily having zero mean. Two contributors to this noise term are the "misadjustment" caused by approximations inherent to the LMS update algorithm and the quantization noise due to the round-off error in the computation and storage of the updated weights. Treichler (ref 4) studied the characteristics of the misadjustment noise and determined that in low SNR it is Gaussian and independent from one weight to the next. Zeidler et al (ref 2) found in experiments with an operational ALE device that for some values of SNR the noise due to quantization and "other effects" was much greater than predicted for the misadjustment noise of the LMS algorithm.

For the purposes of this study, N(k) was assumed to be a zero mean, white, Gaussian random variable. To determine the effect of this additive noise on ALE resolution, series of weight vectors were formed by adding random noise vectors to a previously determined exact weight vector, $W^{\star}(k)$. The resulting spectral functions $|H(\omega)|$ and $Q(\omega)$ were then tested by using Marple's criterion to determine in which instances the two frequencies were resolved.

For the case in which the variance of the weight vector noise σ^2 is zero, one would expect the fraction of resolved spectra to abruptly change from zero to one as the frequency difference of the tones exceeds the limit of resolution. As σ^2 increases, this transition will broaden.

Before examining the results of specific weight vector noise simulations it is appropriate to note the degree of statistical error in determining the fraction of resolved spectra.

The binomial distribution describes the probability of observing m successes out of n tries when the probability of success is p on one try.

The average and variance are given by the relationships

$$\mu = np$$

$$\sigma^2 = np(1-p)$$

For a given value of n, the maximum of σ^2 occurs at $p = \frac{1}{2}$. In this case the rms error in the resulting fraction m/n, is given by $1/(2\sqrt{n})$. For the work presented here $n > 300$, and the resultant rms error is less than 3 percent.

Figures 36–38 demonstrate the effect of introducing noise into the weight vector for signals for which the inherent SNR is respectively 10, 0, and -20 dB. By using an ensemble of 300 random vectors at each value of R_M, the fraction of resolved spectra was determined separately for $|H(\omega)|$ ($\Delta = 1$) and $Q(\omega)$. These figures show the fraction of spectra which were judged "resolved" when using Marple's criterion for various values of R_M.

Figure 36 shows that for high SNR, $|H(\omega)|$ retains a relatively sharp transition between the resolved and unresolved regions while the transition for $Q(\omega)$ is significantly

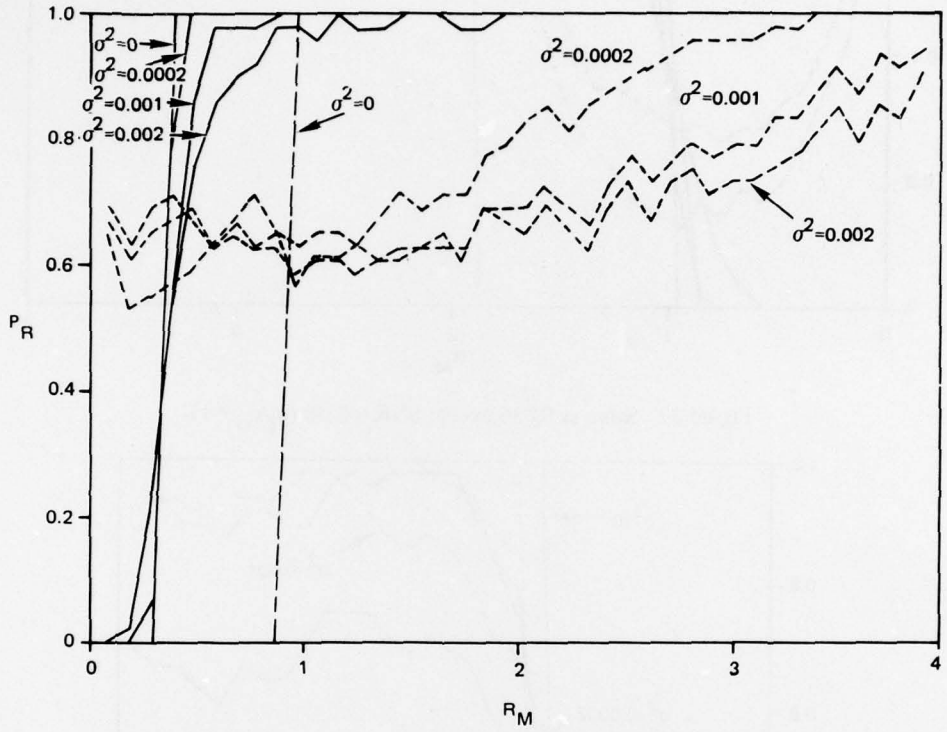

Figure 36. Probability that Marple's criterion will judge a noisy spectrum as resolved for $|H(\omega)|$ (solid) and $Q(\omega)$ (dashed). The signal has SNR = 10 dB (σ_i/σ_0 = 3.16) and ω_{center} = 0.785. The quantity σ_2 represents the variance of the noise added to the ALE weight vector. The ALE had L = 50, Δ = 1.

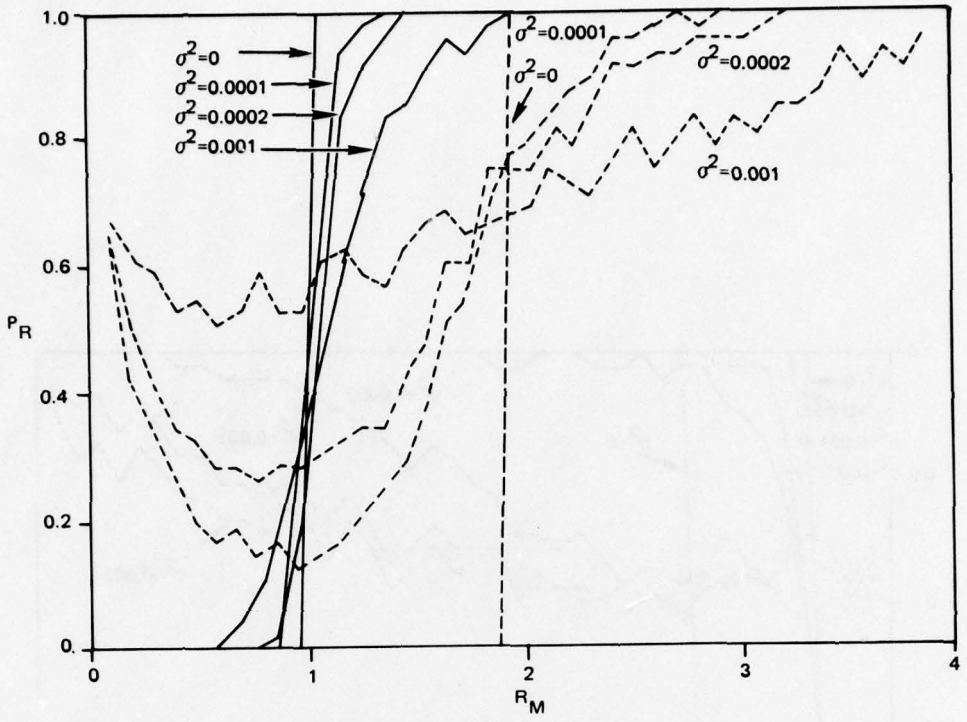

Figure 37. Same as fig 36 except SNR = 0 dB (σ_i/σ_o = 1).

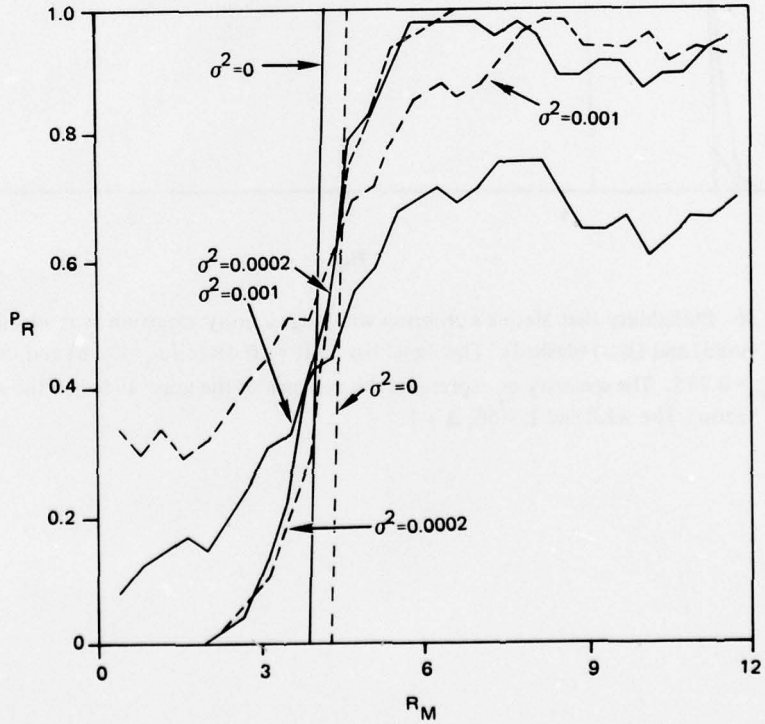

Figure 38. Same as fig 36 except SNR = -20 dB (σ_i/σ_o = 0.1).

distorted even for the smallest values of σ^2. This behavior can be understood by referring to equation 19, repeated here:

$$Q(\omega) = \frac{1}{\left|1 - H^{\star}(\omega)\right|^2}$$

In the high-SNR case, $Q(\omega)$ has very sharp peaks when $H(\omega) = 1$. A small error in $H(\omega)$ near one of these peaks can result in a large percentage error in the quantity $|1 - H^{\star}(\omega)|^2$ and therefore in $Q(\omega)$.

Figure 37 shows the resolution of a 0 dB SNR input signal. In this case the value of R_M at which a particular fraction (0.90 for example) of resolved spectra occurs appears to increase greatly for both $|H(\omega)|$ and $Q(\omega)$. The ratio of the R_Ms denoting $P_R = 0.90$ for $|H(\omega)|$ and $Q(\omega)$ seems to degrade at the same rate as σ^2 is increased.

Figure 38 shows that in the low-SNR case (SNR = -20 dB), $Q(\omega)$ and $|H(\omega)|$ remain essentially the same for low values of σ^2 ($\sigma^2 = 0, 0.0002$), whereas $Q(\omega)$ might be interpreted as being better for higher values of σ^2.

Another aspect of the relative performance of $|H(\omega)|$ and $Q(\omega)$ for high-SNR signals is shown in figure 39. Here the frequency separation and SNR of the two tones were fixed and the fraction of resolved spectra was plotted as a function of σ^2. This figure again shows that with added noise, $Q(\omega)$ degrades faster than $|H(\omega)|$.

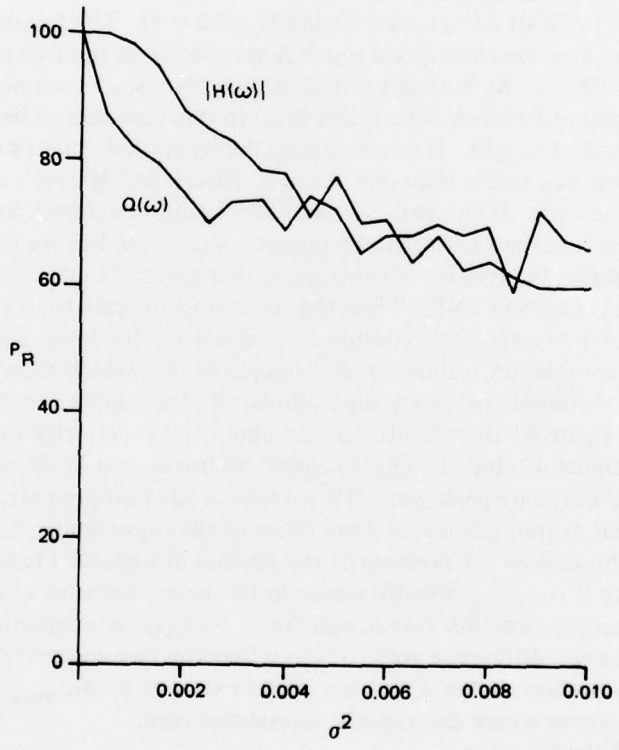

Figure 39. Probabilities that $|H(\omega)|$ ($\Delta = 1$) and $Q(\omega)$ will resolve two tones with $\Delta\omega = 0.2$, $\sigma_i/\sigma_o = 2$, $L = 20$, and $\omega_{center} = 0.785$.

Caution should be used in extending the meaning of these results beyond the limited scope of this study. The effect of input SNR on the covariance of the weight vector noise has been assumed to be small. While this may be the case where quantization noise is dominant, Treichler (ref 4) notes that the misadjustment noise is only white for low SNR. Furthermore, the criterion of resolution used in this report, while very convenient to implement when the exact input frequencies are known, may in fact not be a relevant measure of resolution for the practical case of unknown frequencies. These statements are not intended to depreciate the value of what was done but rather to lay a realistic foundation for its interpretation.

A CRITICAL LOOK AT RESOLUTION CRITERIA

Since the ALE is capable of producing various forms of spectral information ($|H(\omega)|$, $Q(\omega)$, or $S(\omega)$), it is natural to compare their various properties. One must be cautious, however, not to make general conclusions about their relative worth based on one single test. The concept of a "best spectral estimator" may be so dependent on the requirements of a particular application as to be meaningless in the general sense.

The results of the previous section were calculated by using Marple's criterion of resolution. Several examples here presented are to highlight some of the problems that can arise when this criterion is used.

Figure 40 is a plot of $|H(\omega)|$ ($\Delta = 5$) and $S(\omega)(\Delta = 5)$. The frequencies of the two tones marked on the abscissa correspond much more closely to the two peaks in $S(\omega)$ than to the two peaks in $|H(\omega)|$. By Marple's criterion, however, $S(\omega)$ does not resolve the two sinusoids. The judgment between $|H(\omega)|$ and $S(\omega)$ in this case cannot be made independently of the signal information sought. If one is testing the hypothesis that two tones are present at frequencies ω_1 and ω_2 rather than one at ω_{AV}, $|H(\omega)|$ and Marple's criterion may be the most sensitive measure. If the goal is to make an accurate determination of the frequency difference when two tones are known to be present, $S(\omega)$ would prove most effective.

In that example, the relative advantages of two spectral functions were evaluated for specific values of ω_1, ω_2, and SNR. When the ALE must operate for a variety of frequency differences, the choice of a spectral function to characterize the input signal can be further complicated. This complexity is illustrated in figures 41–43, which show $|H(\omega)|$ ($\Delta = 1$) and $Q(\omega)$ for three different frequency separations, all other signal and ALE parameters being the same. In figure 41 there is little doubt about the superiority of $Q(\omega)$ over $|H(\omega)|$. This is still true in figure 42, but the $Q(\omega)$ peaks have broadened noticeably. Figure 43 shows $Q(\omega)$ to have only one peak while $|H(\omega)|$ retains the two-peak structure even though the two peaks appear at frequencies far from those of the input sinusoids.

Figure 44 shows how the position of the peak(s) in a spectral function can change. Plotted in this figure is $\Delta\omega_{meas}$, the difference in frequency between ω_{AV} and the first maximum in the spectral function that occurs for $\omega > \omega_{AV}$, as a function of $\omega_2 - \omega_{AV}$. The measured frequency difference goes to zero where the two spectral peaks have coalesced into one. For the situation shown, $Q(\omega)$ is a better extimate of $\Delta\omega_{meas}$, while $|H(\omega)|$ is better in the small region where $\Delta\omega$ rapidly approaches zero.

In figure 45 the function

$$D(\omega) = \frac{\Delta\omega_{meas} - \Delta\omega}{\Delta\omega} \times 100$$

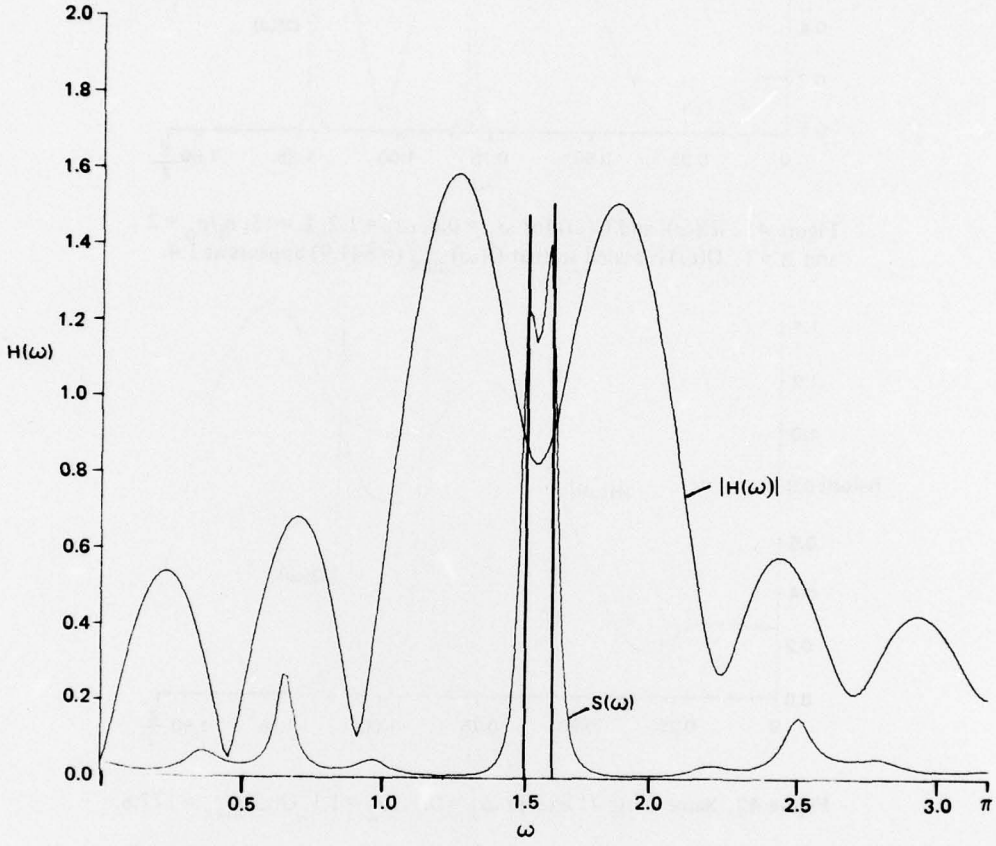

Figure 40. $|H(\omega)|$ and $S(\omega)$ for $\Delta = 5$, $\sigma_i/\sigma_o = 2$, $\omega_1 = 1.5$, $\omega_2 = 1.6$, and $L = 15$. The $S(\omega)$ has been scaled so that $S(\omega)_{max}$ (= 39.7) occurs at 1.4. Note by the extended lines marking ω_1 and ω_2 that $S(\omega)$ is unresolved by Marple's criterion.

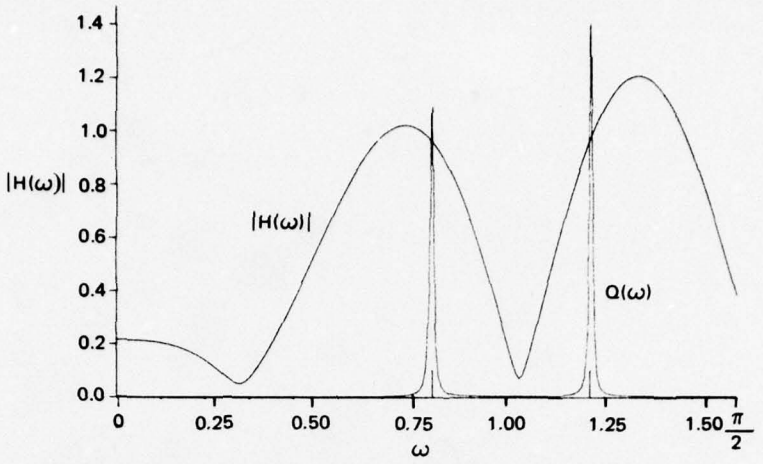

Figure 41. $|H(\omega)|$ and $Q(\omega)$ for $\omega_1 = 0.8$, $\omega_2 = 1.2$, $L = 15$, $\sigma_i/\sigma_o = 2$ and $\Delta = 1$. $Q(\omega)$ is scaled so that $Q(\omega)_{max}$ (= 841.9) appears at 1.4.

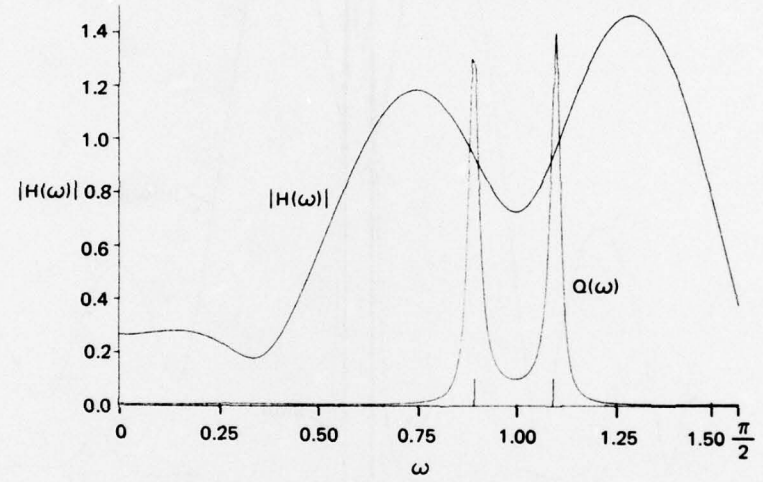

Figure 42. Same as fig 41 except $\omega_1 = 0.9$, $\omega_2 = 1.1$, $Q(\omega)_{max} = 177.8$.

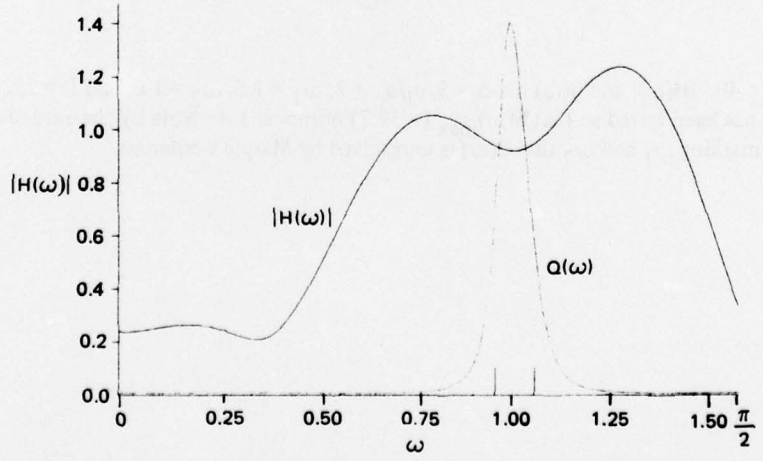

Figure 43. Same as fig 41 except $\omega_1 = 0.95$, $\omega_2 = 1.05$, $Q(\omega)_{max} = 159.3$

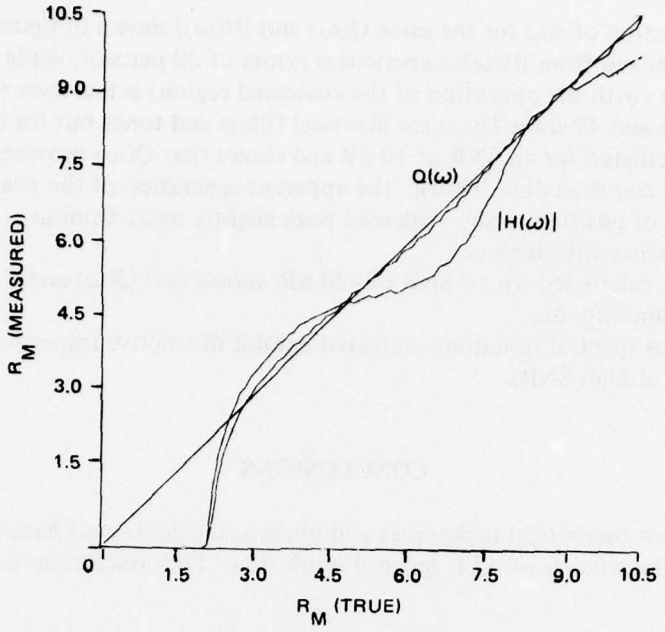

Figure 44. $|\omega_2 - \omega_{AV}|$ as measured by the peak locations of $|H(\omega)|$ and $Q(\omega)$, for $\Delta = 1$, $L = 15$, $\sigma_i/\sigma_0 = 1$, and $\omega_{center} = 1.57$. The R_M (measured) = R_M (true) line is drawn in for reference.

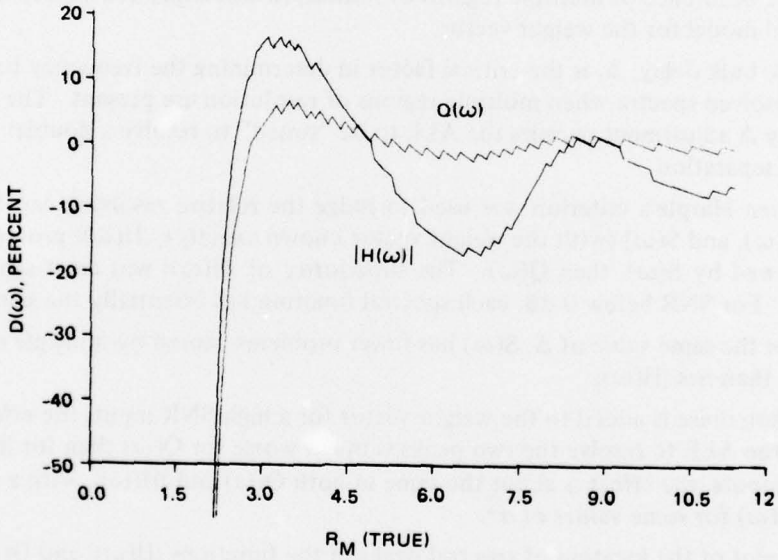

Figure 45. Percent differences between R_M (true) and R_M (measured) for figure 44.

is plotted as a function of $\Delta\omega$ for the same $Q(\omega)$ and $|H(\omega)|$ shown in figure 44. The estimate of $\Delta\omega$ derived from $|H(\omega)|$ experiences errors of 20 percent, while the error of the $Q(\omega)$ estimate (with the exception of the coalesced region) is less than 6 percent.

Figures 46 and 47 show $D(\omega)$ for identical filters and tones but for different SNRs. Figure 46 was calculated for an SNR of 10 dB and shows that $Q(\omega)$ provides a much better estimate of $\Delta\omega$ than does $|H(\omega)|$. the apparent separation of the peaks near $\Delta\omega = 0$ is due to the shift of position of the coalesced peak slightly away from ω_{AV}, caused by the negative frequency interference.

Figure 47, calculated for an SNR of -20 dB, shows that $Q(\omega)$ and $|H(\omega)|$ perform comparably in estimating $\Delta\omega$.

The various spectral functions evaluated exhibit distinctive responses to similar inputs (especially at high SNR).

CONCLUSIONS

A variety of theoretical techniques and numerical calculations have been employed to illuminate the various facets of ALE spectral resolution. The conclusions are summarized as follows:

A modified maximum entropy spectrum ($S(\omega)$) having many of the desirable properties of $Q(\omega)$ can be formed from the ALE weight vector for bulk delay $\Delta \neq 1$.

For $\Delta > 1$, both $|H(\omega)|$ and $S(\omega)$ have multiple regions of resolution, contrary to the concept of a simple limit of resolution.

The occurence of multiple regions of resolution was explained simply in terms of a geometrical model for the weight vector.

The bulk delay, Δ, is the critical factor in determining the frequency bands which result in resolved spectra when multiple regions of resolution are present. The capability of arbitrary Δ adjustment permits the ALE to be "tuned" to resolve a doublet with a known frequency separation.

When Marple's criterion was used to judge the relative resolving capabilities of $|H(\omega)|$, $Q(\omega)$, and $S(\omega)$ (with the weight vector known exactly), $|H(\omega)|$ proved to be the best, followed by $S(\omega)$, then $Q(\omega)$. The superiority of $|H(\omega)|$ was most significant for high SNR. For SNR below 0 dB, each spectral function has essentially the same resolution.

For the same value of Δ, $S(\omega)$ has fewer problems caused by multiple regions of resolution than has $|H(\omega)|$.

When noise is added to the weight vector for a high SNR input, the effect on the ability of the ALE to resolve the two peaks is much worse for $Q(\omega)$ than for $|H(\omega)|$. For low-SNR inputs, the effect is about the same in both $Q(\omega)$ and $|H(\omega)|$, with a slight superiority of $Q(\omega)$ for some values of σ^2.

A plot of the location of spectral peaks in the functions $|H(\omega)|$ and $Q(\omega)$ shows that for higher SNR, the locations of the tonal frequencies correspond much more closely to the peaks of $Q(\omega)$ than to the peaks of $|H(\omega)|$. For low SNR, the performance of the two spectral estimators is about the same.

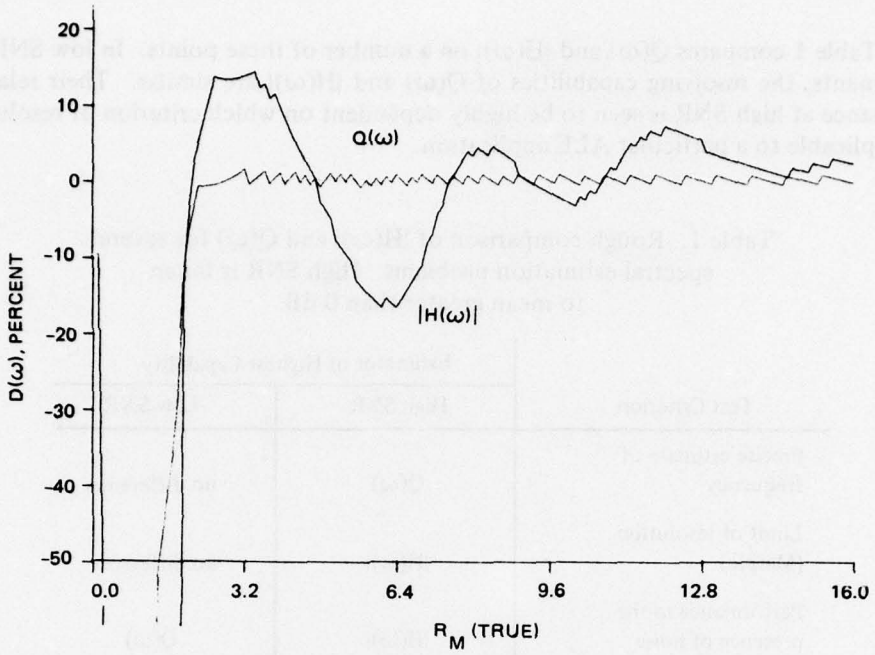

Figure 46. Plot similar to fig 45, for L = 32, σ_i/σ_o = 3.16 (10 dB), Δ = 1, ω_{center} = 1.57.

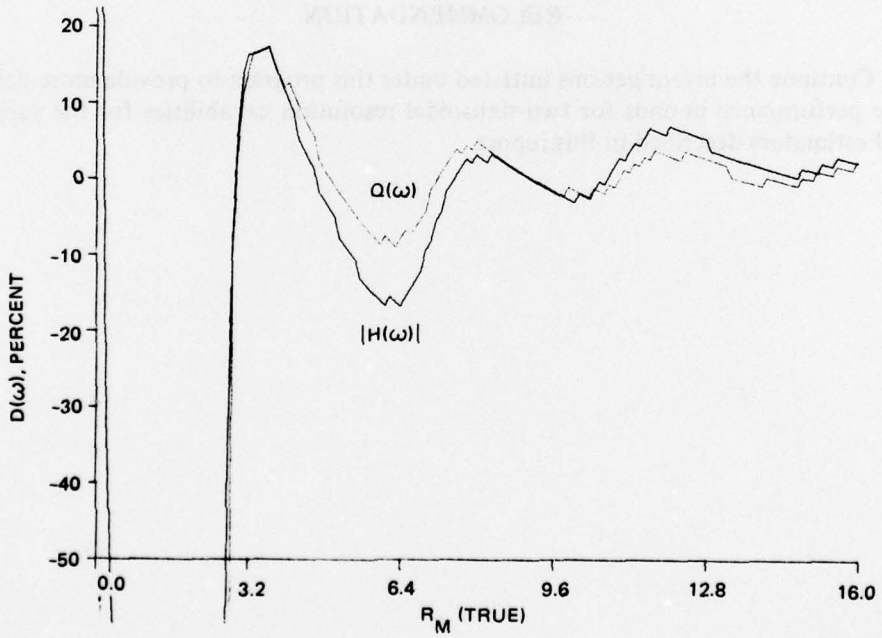

Figure 47. Plot identical to fig 46 except σ_i/σ_o = 0.1 (-20 dB).

Table 1 compares $Q(\omega)$ and $|H(\omega)|$ on a number of these points. In low-SNR signal environments, the resolving capabilities of $Q(\omega)$ and $|H(\omega)|$ are similar. Their relative performance at high SNR is seen to be highly dependent on which criterion of resolution is most applicable to a particular ALE application.

Table 1. Rough comparison of $|H(\omega)|$ and $Q(\omega)$ for several spectral estimation problems. High SNR is taken to mean greater than 0 dB.

	Estimator of Highest Capability	
Test Criterion	High SNR	Low SNR
Precise estimate of frequency	$Q(\omega)$	no difference
Limit of resolution (Marple)	$\|H(\omega)\|$	no difference
Performance in the presence of noise	$\|H(\omega)\|$	$Q(\omega)$
Freedom from multiple regions of resolution	$Q(\omega)$	not evaluated

RECOMMENDATION

Continue the inventigations initiated under this program to provide more definitive baseline performance bounds for two-sinusoidal resolution capabilities for the various spectral estimators described in this report.

REFERENCES

1. Widrow, B, Glover, JR, McCool, JM, Kaunitz, J, Williams, CS, Hearn, RH, Zeidler, JR, Dong, E, and Goodlin, RC, Adaptive Noise Cancelling: Principles and Applications, IEEE Proc, vol 63, p 1692–1716, December 1975.

2. NOSC TR 193, Adaptive Enhancement of Multiple Sinusoids in Uncorrelated Noise, by JR Zeidler, EH Satorius, DM Chabries, and HT Wexler, 1 October 1977. Published later as The Performance of the Adaptive Line Enhancer for Multiple Sinusoidal Inputs in White Noise, IEEE Trans on Acoustics, Speech and Signal Processing, June 1978.

3. NOSC Technical Report NUC TP 530, Principles and Applications of Adaptive Filters: A Tutorial Review, by JM McCool and B Widrow, March 1977.

4. Treichler, J, The Spectral Line Enhancer, PhD dissertation, Dept of Electrical Engineering, Stanford University, Stanford CA, May 1977.

5. Burg, JP, Maximum Entropy Spectral Analysis, paper presented at the 37th Annual International Meeting, Society of Exploration Geophysicists, Oklahoma City OK, 31 October 1967.

6. Widrow, B, Adaptive Filters, in Aspects of Network and System Theory, R Kalman and N DeClaris, Ed, p 563–587, Holt, Rinehart, and Winston, New York NY, 1971.

7. NOSC TR 231, Modified Maximum Entropy Spectral Analysis of Bandlimited Signals In Lowpass Noise, by ST Alexander, 30 April 1978.

8. NOSC TR 232, Linear Predictive Spectral Estimation of Bandlimited Signals in Lowpass Noise, by ST Alexander and EH Satorius, 31 March 1978.

9. Van den Bos, A, Alternative Interpretation of Maximum Entropy Spectral Analysis, IEEE Trans on Information Theory, vol IT-17, p 493–494, July 1971.

10. Ulrych, TJ, and Clayton, RW, Time Series Modelling and Maximum Entropy, Physics of the Earth and Planetary Interiors, vol 12, p 188–200, 1976.

11. Marple, S, Conventional Fourier, Autoregressive, and Special ARMA Methods of Spectrum Analysis, engineering thesis, Department of Electrical Engineering, Stanford University, Stanford CA, 1976.

12. Wold, H, Bibliography on Time Series and Stochastic Processes, Oliver and Boyd, London, 1965.

13. Koopmans, LH, The Spectral Analysis of Time Series, Academic Press, New York NY, 1974.

14. Graupe, D, Krause, DJ, and Moore, JB, Identification of Autoregressive Moving-Average Parameters of Time Series, IEEE Trans on Automatic Control, vol AC-20, p 104–107, February 1975.

15. Peacock, K, and Treitel, S, Predictive Deconvolution: Theory and Practice, Geophysics, vol 34, p 155–169, April 1969.

16. Kailath, T, A View of Three Decades of Linear Filtering Theory, IEEE Trans on Information Theory, vol IT-20, p 145–181, March 1974.

17. Griffiths, LJ, Rapid Measurement of Digital Instantaneous Frequency, IEEE Trans on Acoustics, Speech and Signal Processing, vol ASSP-23, p 207–222, April 1975.

INITIAL DISTRIBUTION

NAVAL ELECTRONIC SYSTEMS COMMAND
PME124-20 (CDR P GIRARD)
NELEX-320 (WS KAMMINGA)
NELEX-320 (CDR A MILLER)

NAVAL SEA SYSTEMS COMMAND
NSEA-06H2 (K WONG)
NSEA-06H1 (J NEELEY)

DEFENSE ADVANCED RESEARCH PROJECTS AGENCY
R GUSTAFSON

ARPA RESEARCH CENTER
UNIT 1
MOFFETT FIELD, CA 94035
RD TRUEBLOOD

ANTI-SUBMARINE WARFARE SYSTEMS PROJECT OFFICE
ASW-13 (RW BRYANT)

APPLIED PHYSICS LABORATORY
JOHNS HOPKINS UNIVERSITY
JOHNS HOPKINS ROAD
LAUREL, MD 20810
CODE S2P (P FUECHSEL)

STANFORD UNIVERSITY
STANFORD, CA 94305
DEPT OF ELECTRICAL ENGINEERING
INFORMATION SYSTEMS LAB
PROF B WIDROW

COLORADO STATE UNIVERSITY
FORT COLLINS, CO 80523
DEPT OF ELECTRICAL ENGINEERING
PROF L SCHARF

UNIVERSITY OF COLORADO
BOULDER, CO 80309
DEPT OF ELECTRICAL ENGINEERING
PROF LJ GRIFFITHS

KANSAS STATE UNIVERSITY
MANHATTAN, KS 66506
DEPT OF ELECTRICAL ENGINEERING
PROF N AHMED

ARGO SYSTEMS
1069 EAST MEADOW CIRCLE
PALO ALTO, CA 94303
M FROST
J TRIECHLER

HYDROTRONICS, INC
3420 KENYON STREET
SUITE 111
SAN DIEGO, CA 92152
M SHENSA

INTERSTATE ELECTRONICS CORP
707 E VERNON AVE
PO BOX 3317
ANAHEIM, CA 92803
J WILLIAMS

ORINCON
PO BOX 22113
SAN DIEGO, CA 92122
JT RICKARD (3)

RAYTHEON
SUBMARINE SIGNAL DIVISION
PORTSMOUTH RI 02871
S KAY

RESEARCH TRIANGLE INSTITUTE
PO BOX 12194
RESEARCH TRIANGLE PARK
NC 27709
E BAXA
J CLAREY

ROCKWELL INTERNATIONAL
MARINE SYSTEMS DIVISION
AUTONETICS GROUP
3370 MIRALOMA AVE
PO BOX 4921
ANAHEIM, CA 92803
M DENTINO
W BURDIC

TRW SYSTEMS, INC
7600 COLSHIRE DRIVE
MC LEAN, VA 22101
W RICHTER

DEFENSE DOCUMENTATION CENTER (12)